ARCHIVES OF ACOUSTICS
5, 3, 191-196 (1980)

ACOUSTIC IMPEDANCE OF AN ISOTROPIC MEDIUM FOR RAYLEIGH WAVES

ALEKSANDER OPILSKI, MARIAN URBAŃCZYK

Institute of Physics, Silesian Polytechnic (44-100 Gliwice)

The acoustic impedance of an isotropic non-piezoelectric medium has been determined for Rayleigh waves. The numerical values of this impedance are very different from the values of the impedance of the medium for a plane bulk wave.

1. Introduction

Analytical solutions of the problems of elastic surface wave propagation are known only for a limited number of half space configurations (Lamb, 1904), and for the simple layered media (Ewing at al. 1957). The problems connected with wave propagation on the surface of a bounded medium containing step discontinuities are complex in so far as it is difficult to give analytical expressions describing the behaviour of Rayleigh waves in these cases. Only the solutions for a single discontinuity (Tuan, 1974) are known. Nevertheless the problem is important in view of the wider application of systems with surface wave containing wave-guide discontinuities in such electronic devices as resonators, bandpass filters, code filters etc.

The properties of complex wave-guides can be easily examined with the use of equivalent circuits. The quantity characterizing a wave-guide medium is the acoustic impedance. The conditions of surface acoustic wave propagation of the Rayleigh type differ from those of plane bulk waves. The characteristic impedance of the medium for this type of wave differs from the analogous quantity for bulk waves.

In this paper, the acoustic impedance of Rayleigh waves in an isotropic, non-piezoelectric medium has been determined.

2. The acoustic impedance of Rayleigh waves in a plane surface layer ($x_3 \to 0$)

Let us assume that the wave propagates in the x_1 direction, in the x_1x_2 plane. The x_3 axis is directed towards the centre of the medium which is isotropic and non-piezoelectric. The component displacements of particles in the medium

from the state of equilibrium will take the form [1]:

$$\begin{aligned} u_1 &= [Aike^{-\alpha x_3} - \beta Be^{-\beta x_3}]e^{i(kx_1-\omega t)}, \\ u_2 &= 0, \\ u_3 &= [-\alpha Ae^{-\alpha x_3} - Bike^{-\beta x_3}]e^{i(kx_1-\omega t)}, \end{aligned} \tag{1}$$

where α, β are decay constants,

$$\alpha^2 = k^2 - \omega^2/a_1^2, \qquad \beta^2 = k^2 - \omega^2/a_2^2, \tag{2}$$

a_1 and a_2 are the velocities of the bulk longitudinal and transverse waves respectively, ω is the angular frequency, and k is the Rayleigh wave number.

Using the condition of the stress vanishing on the free surface of the medium [1],

$$\sigma_{3i} = 0, \tag{3}$$

we shall express amplitude B by amplitude A in formulae (1). The components of stress acting in the medium will have the form:

$$T_1 = \sigma_{11} + \sigma_{31}, \qquad T_2 = \sigma_{22}, \qquad T_3 = \sigma_{13} + \sigma_{33}. \tag{4}$$

In the case of a thin layer ($x_3 \to 0$)

$$T_1 = \sigma_{11}, \qquad T_2 = \sigma_{22}, \qquad T_3 = 0. \tag{5}$$

Denoting the stress tensor by the strain tensor for the isotropic medium [2],

$$\sigma_{ij} = 2\mu\varepsilon_{ij} + \lambda\delta_{ij}\varepsilon_{kk}, \tag{6}$$

where

$$\delta_{ij} = \begin{cases} 1 & \text{for } i = j, \\ 0 & \text{for } i \neq j, \end{cases}$$

and λ, μ are the Lame coefficients, we obtain:

$$\begin{aligned} T_1 &= -(2\mu+\lambda)Ak^2\left[1 - \frac{2\alpha\beta}{k^2+\beta^2}\right]e^{ikx_1} + \lambda A\alpha^2\left[1 - \frac{2k^2}{k^2+\beta^2}\right]e^{ikx_1}, \\ T_2 &= A\lambda\left\{\alpha^2\left[1 - \frac{2k^2}{k^2+\beta^2}\right] - k^2\left[1 - \frac{2\alpha\beta}{k^2+\beta^2}\right]\right\}e^{ikx_1}, \\ T_3 &= 0. \end{aligned} \tag{7}$$

The components of the velocity vector for particles in the medium are:

$$\begin{aligned} v_1 &= \left.\frac{du_1}{dt}\right|_{x_3=0} = A\omega k\left[1 - \frac{2\alpha\beta}{k^2+\beta^2}\right]e^{ikx_1}, \\ v_2 &= \left.\frac{du_2}{dt}\right|_{x_3=0} = 0, \\ v_3 &= \left.\frac{du_3}{dt}\right|_{x_3=0} = Ai\omega\alpha\left[1 - \frac{2k^2}{k^2+\beta^2}\right]e^{ikx_1}. \end{aligned} \tag{8}$$

Denoting the components of the acoustic impedance vector of the medium in the x_1 direction as

$$Za_i = -\frac{T_i}{v_i}, \quad i = 1, 2, 3, \tag{9}$$

we obtain

$$Za_1 = \frac{2\mu+\lambda}{v} - \frac{v\lambda[1-(v/a_1)^2]}{a_2^2[2-(v/a_2)^2-2\sqrt{1-\left(\frac{v}{a_1}\right)^2}\cdot\sqrt{1-\left(\frac{v}{a_2}\right)^2}}, \tag{10}$$

$$Za_2 \to \infty, \quad Za_3 = 0,$$

where v is the Rayleigh wave velocity.

In the case of a bulk longitudinal wave ($v = a_1$), the impedance Za_1 takes the form

$$Za_1 = \frac{2\mu+\lambda}{a_1} = Z_{obj}, \tag{11a}$$

whereas for a bulk transverse wave ($v = a_2$) we have

$$Za_1 = \frac{2\mu+\lambda}{a_2} + \frac{\lambda}{a_2}\left[1-\left(\frac{a_2}{a_1}\right)^2\right], \tag{11b}$$

where Z_{obj} is the acoustic impedance for a bulk wave in the unbounded medium.

Formula (10) shows that value of the impedance medium for a Rayleigh wave is greater than the impedance of the same medium for a bulk wave.

Limiting the medium to a half-space has a bearing on the propagation of the bulk transverse wave ($Za_1 > Z_{obj}$), although it has no influence on the behaviour of the longitudinal wave ($Za_1 = Z_{obj}$).

3. Acoustic impedance of Rayleigh waves in an elastic, isotropic half-space

Let us widen our reasoning, taking into account the fact that a surface wave of the Rayleigh type propagates in a certain layer at the surface of the elastic half-space. In this case the stress components have the form

$$\begin{aligned} T_1 &= A\{\lambda(\xi_1-\xi_2)-2\mu(\xi_2+i\xi_3)\}e^{-\alpha x_3+ikx_1}, \\ T_2 &= A\lambda(\xi_1-\xi_2)e^{-\alpha x_3+ikx_1}, \\ T_3 &= A\{2\mu(\xi_1-i\xi_3)+(\xi_1-\xi_2)\}e^{-\alpha x_3+ikx_3}, \end{aligned} \tag{12}$$

where

$$\xi_1 = \left[1-\frac{2k^2}{k^2+\beta^2}\right]\alpha^2, \quad \xi_2 = \left[1-\frac{2\alpha\beta}{k^2+\beta^2}\right]k^2, \quad \xi_3 = \left[1-\frac{k^2+\alpha\beta}{k^2+\beta^2}\right]k\alpha, \tag{13}$$

while the components of the particle velocity vector in the medium will be the following:

$$v_1 = \frac{A\omega}{k}\,\xi_2 e^{-ax_3+ikx_1},$$

$$v_2 = 0, \tag{14}$$

$$v_3 = \frac{Ai\omega}{a}\,\xi_1 e^{-ax_3+ikx_1}.$$

Applying formulae (12) and (14) we obtain a medium impedance in the x_1 direction:

$$Za_1 = \frac{\lambda+2\mu}{v} - \frac{\lambda\xi_1 - i2\mu\xi_3}{v\xi_2},$$

$$Za_2 \to \infty, \tag{15}$$

$$Za_3 = \frac{a}{\omega\xi_1}\{2\mu\xi_3 + i[(2\mu+\lambda)\xi_1 - \lambda\xi_2]\}.$$

The components of the acoustic impedance vector of the medium become complex when wave penetration inside the medium is considered. The imaginary part of the acoustic impedance represents those modes which do not propagate in the medium [3].

For the bulk longitudinal and transverse waves, the formulae denoting the medium impedance in the x_1 direction (Za_1) are identical to formulae (11) arrived at in section 2, whereas in the x_3, direction, the impedance for the longitudinal waves is infinitely great, while for the transverse waves it has a purely imaginary value.

In the case of CdS, the characteristic impedance for the bulk waves $Za_{obj} = 56 \cdot 10^6\ \Omega$, whereas for the surface waves formulae (15) give the following values of the impedance components:

$$|Za_1| = 97 \cdot 10^6\ \Omega, \qquad |Za_2| = 12 \cdot 10^6\ \Omega.$$

4. Conclusions

Introducing a medium acoustic impedance for surface waves is essential, since the numerical values of this impedance differ considerably from the medium impedance values for the two-dimensional bulk waves. In addition, the acoustic impedance determined for Rayleigh waves has an complex form, which points to different propagating conditions for the Rayleigh modes compared to the bulk modes in an unbounded medium.

References

[1] W. P. Mason, R. S. Thurston, *Physical acoustics, principles and methods*, New York – London 1970, vol. VI. p. 146.
[2] W. Nowacki, *Theory of elasticity* (in Polish), PWN, Warszawa 1970, p. 93.
[3] B. A. Auld, *Acoustic fields and waves in solids*, New York – London, 1973, vol. I, p. 176.

Received on September 5, 1979; revised version on March 1, 1980.

ARCHIVES OF ACOUSTICS
5, 3, 197-220 (1980)

AN ANALYSIS OF PULSED ULTRASONIC TRANSMIT-RECEIVE SYSTEMS FOR MEDICAL DIAGNOSTICS

ANNA MARKIEWICZ

Institute of Physics, Uniwersity of Gdańsk (80-952 Gdańsk, ul. Wita Stwosza 57)

This paper presents a method for the calculation of the shape and size of pulses radiated and received by ultrasonic transmitting-receiving systems used in medical diagnostics. Using an equivalent electrical circuit for the transducer, the transfer functions for different working conditions of the transducer were calculated and, on the basis of these functions the acoustical and electrical behaviour was calculated. Because of the complicated nature of the mathematical relations, continuous Fourier transform (CFT) was used to describe the systems. This was then replaced by a discrete Fourier transform (DFT), thus preparing the relations for numerical calculations. The DFT was in turn calculated using the fast Fourier transform (FFT). Calculations were made for a number of practically realized cases. The paper also gives the results obtained from an analysis of the operation of a transmitting transducer for different types of acoustic matching, for a wedged transducer, and for a divided one.

Introduction

An intensively increasing interest in the ultrasonic methods used in medicine can now be observed all over the world. Medical applications require increasingly better diagnostic apparatus. This involves the problem of constructing ultrasonic transmitting-receiving systems which include an electrical transmitter, broad-band transducers, and an electrical receiver. This problem is closely connected with the problems of transient states in piezoelectric transducers.

Since a mathematical description of a transducer in a transient state is quite complicated, papers devoted to this problem do not exhaust the possibilities of definning the optimum design of acousto-electronic systems for the generation and detection of short ultrasonic pulses.

The transient state in a transducer, which results from its large Q – factor and a simultaneous lack of matching to the medium, plays an important role in the problems of signal resolution and the more exact measurement of distance.

The aim of the present work was the design of a method for calculation of the shape and size of the pulses in ultrasonic transmitting-receiving systems used in medical diagnostic apparatus, and to apply this method to a number of practically realized cases.

Analytical method

One of methods for the analysis of the performance of ultrasonic transducers is based on the use of the equivalent electrical circuits of the transducer, and the investigation, on this basis, of the relations between the input and the output [5, 8]. The transducer can then be represented as an electric four-pole network. Irrespective of the inner structure of the system, the work of a linear four-pole network in a steady state, can be characterized by two output and two input quantities, interlinked by linear relations. On the basis of these relations, the transfer function, H, of the four-pole network (which can be used subsequently for the investigation of transient states), may be determined.

For any excitation $f_{we}(t)$, under zero initial conditions, the output signal $f_{wy}(t)$ is defined by the relations [3, 15]: after Laplace transform, it has the form

$$f_{wy}(t) = \alpha^{-1}\{H(s)\cdot F_{we}(s)\},$$

where

$$F_{we}(s) = \alpha\{f_{we}(t)\}, \tag{1}$$

or, after Fourier transform,

$$f_{wy}(t) = \mathscr{F}^{-1}\{H(f)\cdot F_{we}(f)\},$$

where

$$F_{we}(f) = \mathscr{F}\{f_{we}(t)\}. \tag{2}$$

In the present paper, the Laplace transform was used for the simpler cases where the possibility of analytical calculation of the relations existed, whereas Fourier's transform, using the insertion $s = j\omega = j\cdot 2\pi f$, was used for the more complicated cases.

In the determination of the inverse Fourier transforms, the confinuous Fourier transform (CFT) was replaced by the discrete transform (DFT), using the relations describing the continuous and discrete transform and sampling theory [1, 3] (see Appendix). The DFT was subsequently calculated numerically, using the FFT algorithm (Fast Fourier Transform).

Assumptions

An electrical transmitter with an input impedance Z_n is taken to excite the transmitting transducer with the voltage E_n. This transducer radiates an acoustic force F_n into a biological medium. It was assumed that the biological medium did not introduce damping and had an acoustic impedance of $1.5 \cdot 10^6$ kg/m^{2}s (soft tissue is the most frequently investigated biological medium, for which this is the first approximation). The receiving transducer was placed in the near field of the transmitting transducer. In consequence, acoustic field problems were eliminated from the considerations. Diffraction losses were also neglected. It was assumed that this transducer receives the acoustic force F_{od} and converts it to a voltage E_{od} which is the input signal of the electric receiver which has an input impedance z_{wej}.

The analysis of the electrical systems of the transmitter and the receiver was performed using the theory of circuits, based on the designs of the ultrasonograph and ultrasonocardiograph developed in the Department of Ultrasonics IPPT PAN, with subsequent linearization. The phenomena occurring in the electrical receiver were not considered, its effect being limited to that of the first degree input impedance on the behaviour analyzed. The parameters of the tables connecting the transducers with the receiver and the transmitter were also considered.

For comparison of the sizes of the pulses generated by individual transmitting-receiving (T-R) systems, the criterion of the power of the signal received should be used. Since the comparison was performed at a fixed value of electric resistance loading the transducer, a voltage scale was used. This is particularly appropriate since the shapes of the pulses are observed on the oscilloscope screens of diagnostic devices in the forms corresponding to voltages. The time interval, after which the instantaneous value of the signal falls to 10 % of the maximum value, was assumed as pulse duration, although this criterion can be disputed in the case of very irregular pulse shapes.

Transmitting transducer

Fig. 1 shows an equivalent circuit for the transmitting transducer, vibrating in a thickness mode, with consideration of the exciting source and the shunt coil L_0. Transforms of the input quantities are connected with the transforms of the output quantities by the relation

$$\begin{bmatrix} \bar{E}_n \\ \bar{I}_n \end{bmatrix} = [A^n] \begin{bmatrix} \bar{F}_n \\ \bar{V}_n \end{bmatrix}, \tag{3}$$

where $\bar{E}_n$ and $\bar{I}_n$ are transforms of voltage and current, and $\bar{F}_n$ and $\bar{V}_n$ those of force and velocity. $[A^n]$ is a matrix describing the electric system.

On the basis of equation (3), the transfer function of the transmitting system can be determined [5],

$$\bar{E}_n = A_{11}^n \bar{F}_n + A_{12}^n \bar{V}_n, \tag{4}$$

since $\bar{F}_n/\bar{V}_n = z_B A_0$, where z_B is the impedance of the biological medium,

$$H_n(s) = \frac{V_n}{E_n} = \frac{1}{A_{11}^n z_B A_0 + A_{12}^n}. \tag{5}$$

Knowing, in turn, the transfer function, the response of the system to any excitation can be determined, using relation (1) or (2).

Two extreme cases, for which the input electric impedance of the generator is either very large or very small, were assumed as the first approximations to the operation of the transmitting transducer itself (without the compensating inductance).

In the first case the compensation of clamped capacities C_0 and $-C_0$ occurs (when the electrical terminals are open), with the matrix $[A^n]$ assuming the form

$$[A^n] = \begin{bmatrix} \frac{1}{N} & 0 \\ 0 & N \end{bmatrix} \begin{bmatrix} a_{11} & a_{12} \\ a_{21} & a_{22} \end{bmatrix}, \tag{6}$$

where (Fig. 1)

$$\begin{aligned} N &= hC_0 = \sqrt{2f_0 C_0 \varrho_0 c_0 A_0}, \\ a_{11} &= [(m_A+1)e^{s\tau_0} - (m_A-1)e^{-s\tau_0}]/M, \\ a_{12} &= z_0 A_0 [(m_A+1)e^{s\tau_0} + (m_A-1)e^{-s\tau_0}]/M, \\ a_{21} &= (e^{s\tau_0} - e^{-s\tau_0})/(z_0 A_0 M), \\ a_{22} &= [(m_A+2)e^{s\tau_0} - (m_A-2)e^{-s\tau_0} - 4]/M, \\ M &= (m_A+1)e^{s\tau_0} - (m_A-1)e^{-s\tau_0} - 2, \\ m_A &= z_A/z_0. \end{aligned} \tag{7}$$

Inserting relations (6) and (7) into relation (5) we get the function

$$\begin{aligned} H_n(s) = V_0 &[(m_A+1)e^{s\tau_0} - (m_A-1)e^{-s\tau_0} - 2] \times \\ &\times [(m_A+1)(m_B+1)e^{s\tau_0} - (m_A-1)(m_B-1)e^{-s\tau_0}]^{-1}; \\ V_0 &= N/z_0 A_0, \quad m_B = z_B/z_0. \end{aligned} \tag{8}$$

If we consider the excitation $\mathbf{1}(t)$ on the electrical side, then, after using relation (1), we obtain relation (9), defining the wave of acoustic velocity:

$$\begin{aligned} V(t) = V_0 \Big\{ &\frac{1}{m_B+1} \mathbf{1}(t) - \frac{2}{(m_A+1)(m_B+1)} \mathbf{1}(t-\tau_0) - \\ &- \frac{2(m_A-1)}{(m_A+1)^2(m_B+1)} \mathbf{1}(t-2\tau_0) + \ldots \Big\}. \end{aligned} \tag{9}$$

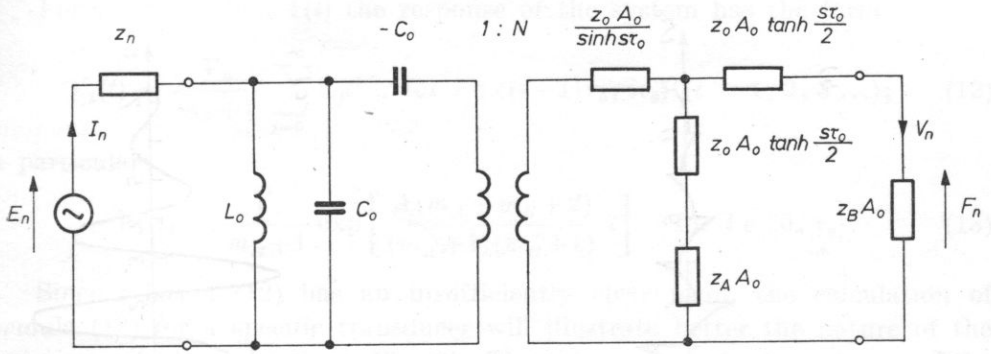

Fig. 1. An equivalent circuit for a piezoelectric transmitting transducer (after Mason) and its electric supply circuit

$z_0 = \varrho_0 c_0$, $z_A = \varrho_A c_A$, $z_B = \varrho_B c_B$ are the acoustic impedances of the transducer, backing load, and the biological medium, respectivelly; c_0 is the ultrasonic wave velocity in the transducer for an electric displacement equal to zero, A_0 is the area of the transducer, $N = hC_0 = \sqrt{2 f_0 C_0 \varrho_0 c_0 A_0}$, $\tau_0 = 1/2f_0$ is the passage time taken for an ultrasonic wave to pass through the open-circuit transducer, f_0 is the frequency of the mechanical resonance, h is a piezoelectric constant, C_0 is the clamped capacity, E_n, I_n are the voltage and current supplying the transducer, z_n is the output impedance of the electrical transmitter, and F_n, V_n are the acoustic force and velocity generated by the transducer

Fig. 2a is an illustration of the result. The response of the system depends only on the purely mechanical properties of the transducer. On both faces: transducer – backing and transducer – biological medium, reflections from the mechanical impedances and partial radiation of the wave into the medium [6] occur every τ_0, i.e. subsequent waves are radiated every τ_0, which have the shape of the excitation. As a result of superposition of these waves an acoustic signal occurs.

In the second case, when the transducer is excited from a generator with very small output impedance, the matrix $[A^n]$ has the form:

$$[A^n] = \begin{bmatrix} 1 & -\frac{1}{sC_0} \\ sC_0 & 0 \end{bmatrix} \begin{bmatrix} \frac{1}{N} & 0 \\ 0 & N \end{bmatrix} \begin{bmatrix} a_{11} & a_{12} \\ a_{21} & a_{22} \end{bmatrix}, \tag{10}$$

with the transfer function for such a transducer being thus given by relation (11),

$$H_n(s) = V_0[(m_A+1)e^{s\tau_0} - (m_A-1)e^{-s\tau_0} - 2] \times$$
$$\times \left\{(m_A+1)(m_B+1)e^{s\tau_0} - (m_A-1)(m_B-1)e^{-s\tau_0} - \right. \tag{11}$$
$$\left. - \frac{A}{s}[(m_A+m_B+2)e^{s\tau_0} - (m_A+m_B-2)e^{s\tau_0} - 4]\right\}^{-1},$$

where

$$A = \frac{N^2}{z_0 A_0 C_0}, \qquad V_0 = \frac{N}{z_0 A_0}.$$

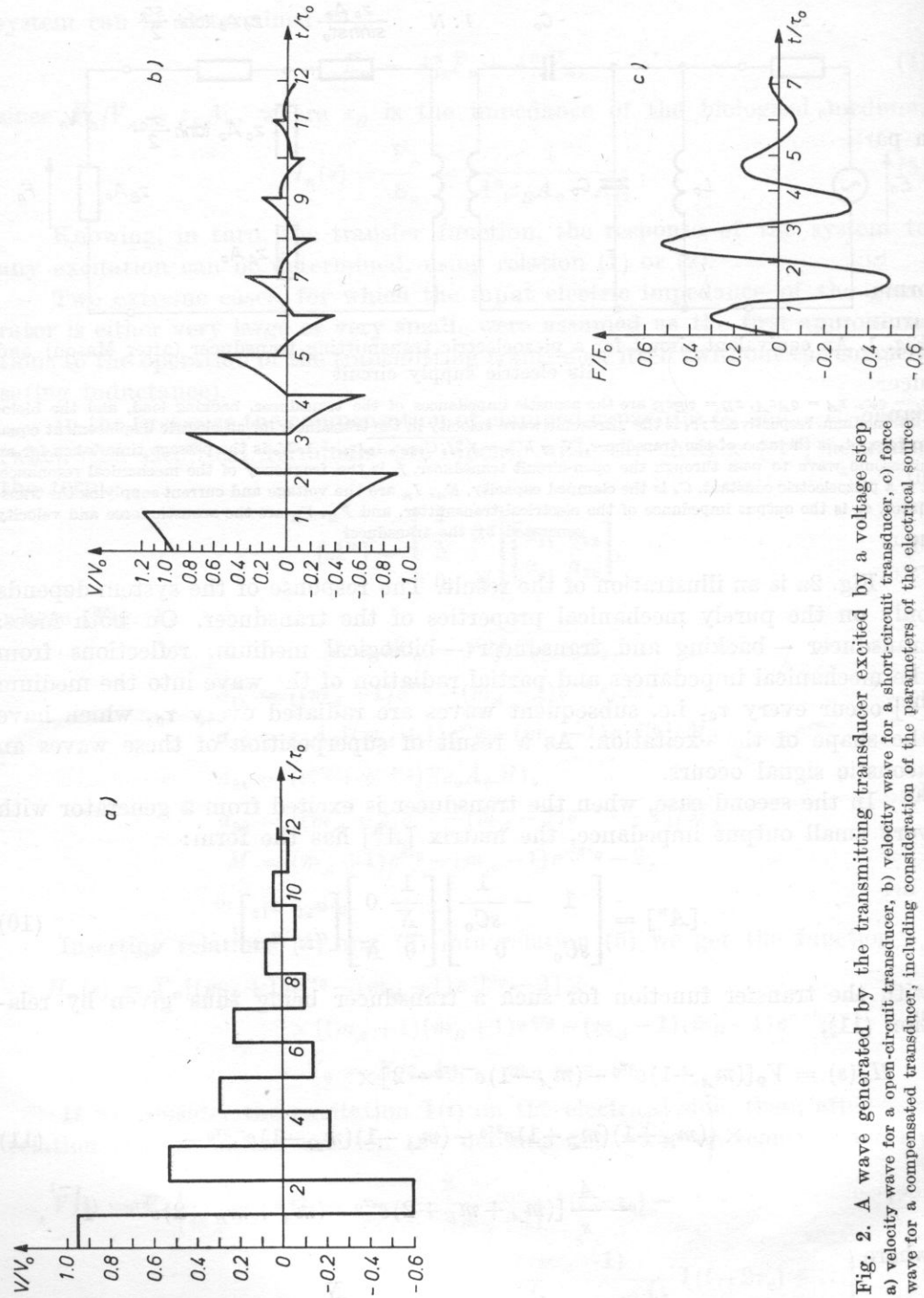

Fig. 2. A wave generated by the transmitting transducer excited by a voltage step
a) velocity wave for a open-circuit transducer, b) velocity wave for a short-circuit transducer, c) force wave for a compensated transducer, including consideration of the parameters of the electrical source

For the excitation $\mathbf{1}(t)$ the response of the system has the form

$$V_i(t) = \frac{V_0}{m_B+1} \sum_{j=0}^{\infty} b_{ij} t^j \quad \text{for } t \in \langle (i-1)\tau_0, i\tau_0) \ (i = 1, 2, 3 \ldots); \tag{12}$$

in particular

$$V_1(t) = \frac{V_0}{m_B+1} \exp\left[\frac{A(m_A+m_B+2)}{(m_A+1)(m_B+1)}\, t\right] \quad \text{for } t \in \langle 0, \tau_0). \tag{13}$$

Since relation (12) has an insufficiently clear form, the calculation of formula (12) for a specific transducer will illustrate better the nature of the variation, which is shown in Fig. 2b. The response of the transducer to the excitation $\mathbf{1}(t)$ is a sum of the purely mechanical response (open-circuit transducer – (9)) and of some additional function, which is responsible for the change of shape from the rectangular. Pulses are generated every τ_0 on both surfaces of the transducer, but they no longer have the shape of the excitation, but rather a shape which depends on the effect of the electrical side of the equivalent circuit of the transducer on the mechanical side. For a time $t \in \langle 0, \tau_0)$, the response of the transducer is given by relation (13). Analogously to electrical systems, the idea of a time constant can be introduced,

$$\tau' = R'C' = \frac{(m_A+1)(m_B+1)}{A(m_A+m_B+2)} = \frac{(R_A+R_0)(R_B+R_0)}{R_A+R_B+2R_0}\left(\frac{-C_0}{N^2}\right), \tag{14}$$

where $R_0 = z_0 A_0$, $R_A = z_A A_0$, and $R_B = z_B A_0$ are acoustic impedances, i.e.

$$R' = (R_A+R_0) \| (R_B+R_0)$$

(the transducer acts as such a resistance for $t \in \langle 0, \tau_0)$;

$$C' = C_0/N^2$$

(a negative capacitance transformed to the mechanical side).

Since $\tau' < 0$, the output for $t \in \langle 0, \tau_0)$ will increase exponentially, with a time constant for this increase equal to $R'C'$.

With consideration of the electrical source and the shunt coil L_0 (which compensates C_0 at the frequency f_0), we have

$$[A^n] = \begin{bmatrix} 1+\dfrac{z_n}{sL_0} & z_u \\ \dfrac{1}{sL_0} & 1 \end{bmatrix} \begin{bmatrix} 1 & -\dfrac{1}{sC_0} \\ sC_0 & 0 \end{bmatrix} \begin{bmatrix} \dfrac{1}{N} & 0 \\ 0 & N \end{bmatrix} \begin{bmatrix} a_{11} & a_{12} \\ a_{21} & a_{22} \end{bmatrix}, \tag{15}$$

while the transfer function of the transmitting transducer becomes:

$$H_n(s) = m_B N[(m_A+1)e^{s\tau_0} - (m_A-1)e^{-s\tau_0} - 2] \times$$

$$\times \left\{\left(1+\frac{z_n}{sL_0}+z_n sC_0\right)[(m_A+1)(m_B+1)e^{s\tau_0} - (m_A-1) \times \right.$$

$$\times (m_B-1)e^{-s\tau_0}] - \frac{A}{s}\left(1+\frac{z_n}{sL}\right)[(m_A+m_B+2)\times$$

$$\times e^{s\tau_0} - (m_A+m_B-2)e^{-s\tau_0} - 4]\Big\}^{-1}. \qquad (16)$$

Fig. 2c shows the wave of force generated by the same transducer as before, but this time including the parameters of the transmitter, according to formula (16), with the excitation, as before, of a voltage step. In this case multiple reflections depend on the impedance "seen" an the borders of the transducer. This impedance is formed by both mechanical and electrical elements, with the shape of response ultimately obtained depending on the superposition of the waves occurring as a result of multiple reflections. The calculation results shown in Fig. 2, were obtained for a transducer with the parameters: $z_0 = 27.0\cdot 10^6$ kg/m^{2}s, $z_A = 6.3\cdot 10^6$ kg/m^{2}s, $f_0 = 2.13$ MHz, $C_0 = 1730$ pF, and a diameter of 2 cm; while, for the case in Fig. 2c, $z_n = 100\ \Omega$ was assumed.

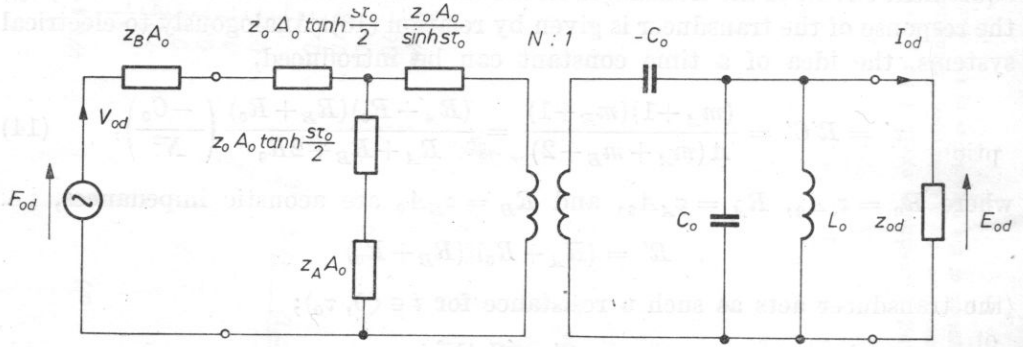

Fig. 3. An equivalent circuit for the receiving transducer

F_{od}, V_{od} are the acoustic force and velocity exciting the transducer, E_{od}, I_{od} are the voltage and current generated by the transducer, and z_{od} is the imput impedance of the electrical receiver

The circuit of the receiving transducer loaded by the electric impedance z_{od} is shown in Fig. 3. The relations describing the system are given by formulae (17) and (18):

$$\begin{bmatrix} \bar{F}_{od} \\ \bar{V}_{od} \end{bmatrix} = [A^{od}] \begin{bmatrix} \bar{E}_{od} \\ \bar{I}_{od} \end{bmatrix}, \qquad (17)$$

where

$$[A^{od}] = \begin{bmatrix} 1 & zA_0 \\ 0 & 1 \end{bmatrix} \begin{bmatrix} a_{22} & a_{12} \\ a_{21} & a_{11} \end{bmatrix} \begin{bmatrix} N & 0 \\ 0 & \frac{1}{N} \end{bmatrix} \begin{bmatrix} 0 & \frac{-1}{sC_0} \\ sC_0 & 1 \end{bmatrix} \begin{bmatrix} 1 & 0 \\ \frac{1}{sL_0} & 1 \end{bmatrix}. \qquad (18)$$

The transfer function of the receiving system was obtained from (17)

and (18), in the form:

$$H_{od}(s) = \frac{\bar{E}_{od}}{\bar{F}_{od}} = \frac{z_{od}}{A_{11}^{od} z_{od} + A_{12}^{od}} = \frac{N z_{od}}{z_0 A_0} [(m_A+1)e^{s\tau_0} -$$

$$-(m_A-1)e^{-s\tau_0} - 2] \left\{ (sC_0 z_{od} + \frac{z_{od}}{sL_0} + 1) [(m_A+1)(m_B+1)e^{s\tau_0} - \right.$$

$$-(m_A-1)(m_B-1)e^{-s\tau_0}] - \frac{A}{s}\left(1 + \frac{z_{od}}{sL_0}\right) [(m_A+m_B+2)e^{s\tau_0} -$$

$$\left. -(m_A+m_B-2)e^{-s\tau_0} - 4] \right\}^{-1}. \tag{19}$$

The transfer function of the receiving transducer $H_{od}(s)$ has the same form as the transfer function of the transmitting transducer; a similar shape for the voltage being generated by the receiving transducer, as for the shape of the force generated by the transmitting transducer (see Fig. 2c).

The transmitting-receiving system

If we consider the transmitting-receiving system described in the assumptions, then the transfer function of such a system is given by the formula

$$H(s) = \frac{\bar{E}_{od}}{\bar{E}_n} = 2H_n(s)H_{od}(s), \tag{20}$$

where $H_n(s)$ and $H_{od}(s)$ are defined by (16) and (19), respectively. On the basis of these relations, the behaviour of the receiving transducer in any T-R arrangement and for any transducer, can be calculated.

The effect of the shape of the excitation on the shape of the voltage obtained for a transducer with the parameters $z_0 = 25 \cdot 10^6$ kg/m^{2}s, $f_0 = 2.72$ MHz, $C_0 = 1260$ pF, loaded at the back with an acoustic impedance of $z_A = 6.1 \cdot 10^6$ kg/m^{2}s, compensated with an inductance L_0, and shunted in the transmitter with the resistance $R = 6.8$ kΩ, was analyzed for the T-R system of the ultrasonograph. All the results presented subsequently in this paper, with the exception of those for the divided transducer, are presented for a transducer with the parameters given above. The amplitude of the exciting voltage was 250 V.

A Heaviside function was assumed as the first approximation to the shape of the excitation

$$E_n(t) = -E_0 \cdot \mathbf{1}(t) \tag{21}$$

with the results being shown in Fig. 4a.

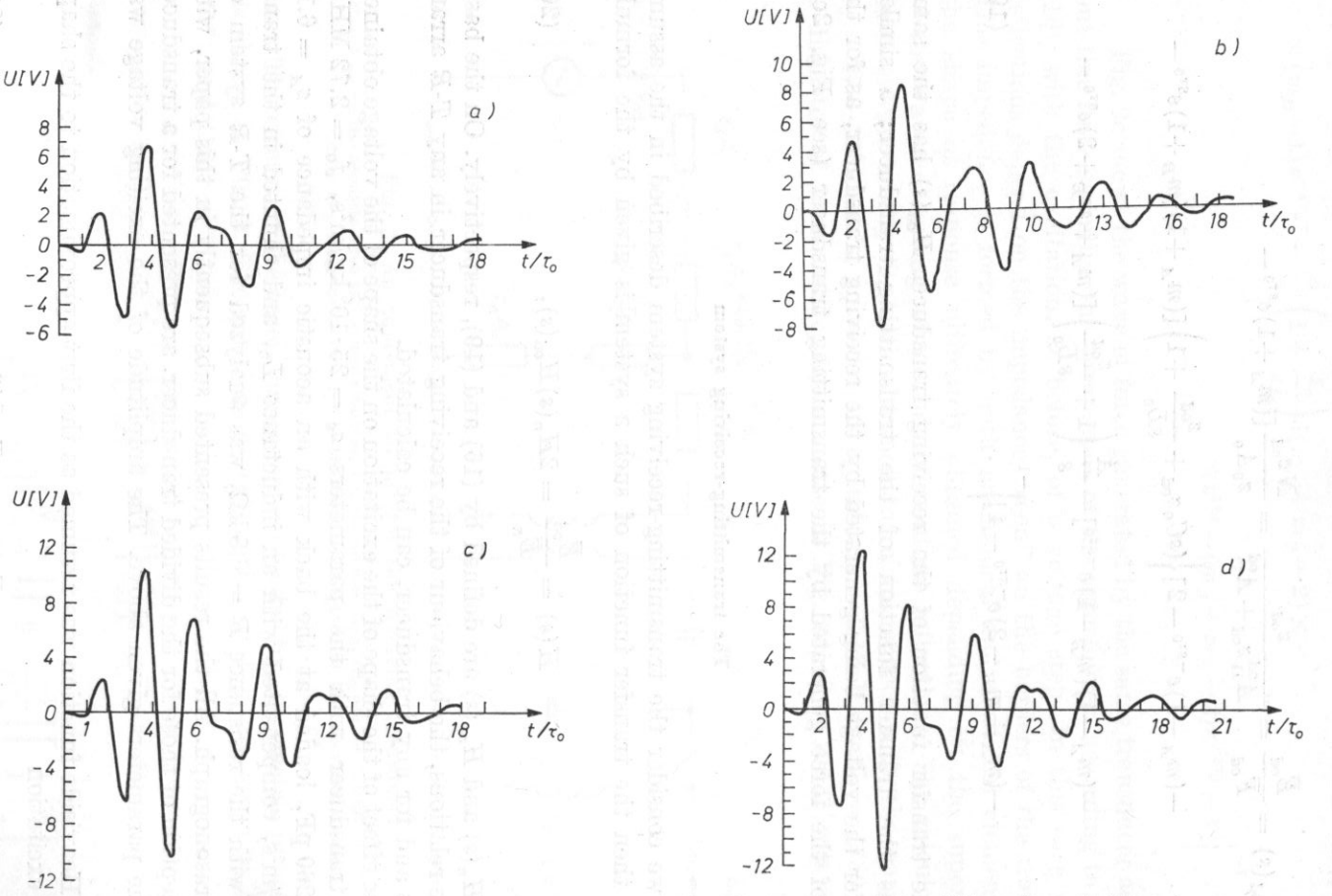

Fig. 4. Voltage received in the T-R system of the ultrasonograph for different excitations

a) a Heaviside time function, b) a linear increase in time to a constant value, c) a rectangular pulse of width τ_0, d) a trapezoidal pulse

As the actual excitations in the ultrasonograph have a finite rise time, an excitation closer to reality, which is described by the following function, was considered as the second excitation:

$$E_n(t) = \begin{cases} \dfrac{-E_0}{\tau_0} t & \text{for } t < \tau_0, \\ -E_0 & \text{for } t \geqslant \tau_0. \end{cases} \tag{22}$$

The shape of voltage obtained for this type of excitation is shown in Fig. 4b. In the case of excitation with a rectangular pulse of width τ_0,

$$E_n(t) = -E_0[\mathbf{1}(t) - \mathbf{1}(t-\tau_0)], \tag{23}$$

the response of the system has the form shown in Fig. 4c, and that for a trapezoidal pulse of duration τ_0 and decreasing from a value E_0 to $\frac{3}{4} E_0$,

$$E_n(t) = \begin{cases} -E_0\left(-\dfrac{t}{4\tau_0} + 1\right) & \text{for } t < \tau_0, \\ 0 & \text{for } t \geqslant \tau_0, \end{cases} \tag{24}$$

is shown in Fig. 4d.

A number of excitation types (a rectangular pulse of duration $2\tau_0$, a double Heaviside function, a trapezoidal pulse) have also been analyzed, but this paper gives only the results which are more interesting from a practical point of view.

The shape of the pulse obtained depends on the multiple reflections occurring as a result of a lack of matching of the transducer on both electrical and acoustical sides. The excitation of the transmitting transducer causes the generation of an acoustical pulse whose shape is different from the shape of the excitation. The acoustic behaviour is the result of the superposition of successive waves generated every τ_0. In turn, the acoustical signal causes the generation of an electrical signal by the receiving transducer.

Since a number of changes occur in the instantaneous value of the acoustic behaviour, each causing the generation of a number of waves in the receiving transducer, the duration of the signal received increases even more.

In a diagnostic apparatus the signal received should have as large an amplitude and as short a duration as possible. A change in the onset time between the limits $0 < t < \tau_0$ affects the amplitude of the signal received, having, however, no larger effect on the duration. It follows from the calculations performed that the largest amplitude is obtained for excitation with a rectangular pulse of width τ_0 (see Table 1).

Illustration of the effect of the resistance shunting the head in the transmitter was analyzed for the ultrasonocardiograph system in which it is possible to adjust this resistance. A $\mathbf{1}(t)$ of amplitude of 600 V was assumed as an excitation. The results presented in Figs. 5a,b,c are for $R = 3.3$ kΩ, 110 Ω, and 20 Ω, respectively. The following conclusion can be drawn on the basis of the

Table 1. Parameters of the voltage pulse received in the T-R system for different excitations

No.	shape of exciting voltage	maximum voltage received U_{max}[V]	duration t [s]	Fig.
1	a Heaviside time function	6.8	13.8 τ_0	4a
2	a linear increase to a constant value	8.8	13.9 τ_0	4b
3	a rectangular pulse of width τ_0	12.5	13.7 τ_0	4c
4	a trapezoidal pulse of witdh τ_0	10.9	13.0 τ_0	4d

results obtained: the durations of the transmitted and received pulses can be changed by a change in the shunting resistance. However, an optimum value of shunting resistance exists, for which the duration will decrease if a suitable sensitivity of the head is preserved (see Table 2). The shape of the pulse generated also changes. A component of higher frequency, which is difficult to explain, occurs for a low value of the shunting resistance R.

Table 2. Duration of the pulse received in the T-R system for different shunting resistances

No.	shunting resistance R	duration t [s]	Fig.
1	ultrasonograph 6.8 kΩ	13.8 τ_0	4a
2	ultrasonocardiograph 3.3 kΩ	17.9 τ_0	5a
3	110 Ω	10 τ_0	5b

The effect of acoustic loads

Since a large mismatch occurs between the transducer and the biological medium, the possibility of improving the operating conditions on the acoustical side was analyzed.

One solution may be the introduction of a matching layer between the transducer and the biological medium.

The requirements for matching are that the layer should have a thickness of $\lambda/4$ and an acoustic impedance equal to the geometrical mean of the impe-

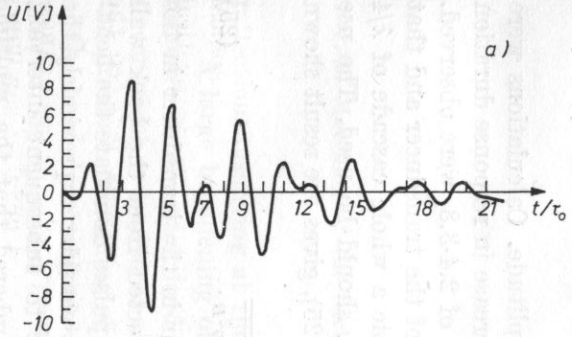

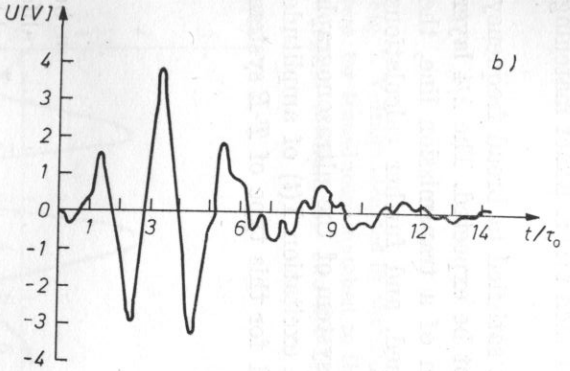

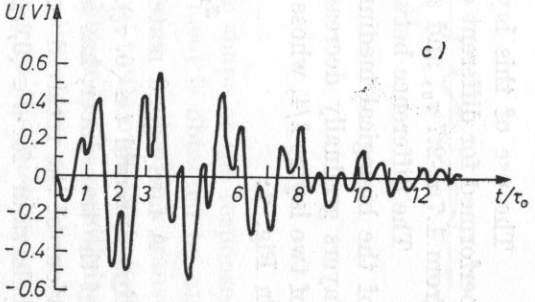

Fig. 5. Voltage received in the ultrasonocardiograph system, for an excitation $\mathbf{1}(t)$ of amplitude 600 V, for different shunting resistances
a) $R = 33\ \text{k}\Omega$, b) $R = 110\ \Omega$, c) $R = 20\ \Omega$

dances to be matched [4, 13]. A $\lambda/4$ layer best matches those two media hwose impedances are real and only slightly different from each other. Exact matching occurs for one frequency only.

In the present case, these conditions are not satisfied (a broad frequency band is used) and therefore ideal matching cannot be expected. The $\lambda/4$ layer was included in the equivalent circuits in the form of a transmission line, the transfer functions the T-R system [13] determined, and further calculations performed.

Fig. 6 shows the voltage received in the T-R system of the ultrasonograph working with transducers with $\lambda/4$ layers with an excitation $\mathbf{1}(t)$ of amplitude 250 V. Further results presented were calculated for this type of T-R system with $\mathbf{1}(t)$ excitation.

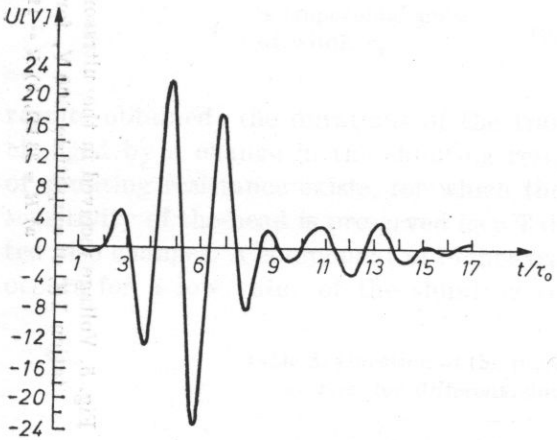

Fig. 6. Voltage received in the T-R system for transducers with a $\lambda/4$ layer, for the excitation $\mathbf{1}(t)$

The use of this layer mainly improves the amplitude. Calculations were performed for different excitation types. A slight decrease in response duration from 1.7 τ_0-2.7 τ_0, and amplitudes larger by a factor of 2.4-3.8, were observed.

The difference between the acoustic impedance of the transducer and that of the biological medium is so large that in principle a whole cascade of $\lambda/4$ layers gradually decreasing the acoustic impedance, should be used. The use of two layers $\lambda/4$, whose impedance satisfy relations (25), gives the result shown in Fig. 7:

$$z_1 = \sqrt{z_0\sqrt{z_0 z_B}}, \qquad z_2 = \sqrt{z_B\sqrt{z_0 z_B}}. \tag{25}$$

A fairly good matching occurs for the behaviour in the transducer in the time interval $t \in \langle 0, \tau_0)$. Matching to the wave reflected from the back wall of the transducer, has also been assured. These two pulses dominate the behaviour of the received voltage, while in the two cases considered previously the behaviour for $t \in \langle 0, \tau_0)$ was very small compared to subsequent intervals, sometimes even $U < 10\%\, U_{\max}$. It should be remembered that the multiple

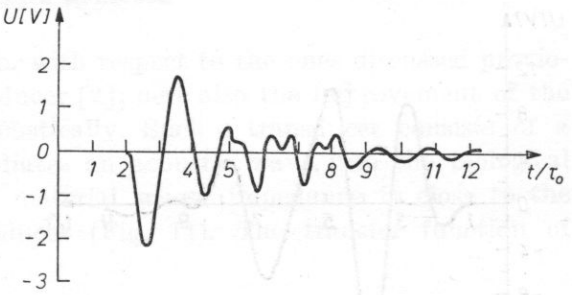

Fig. 7. Voltage received in the T-R system for transducers matched to the biological medium by two $\lambda/4$ layers

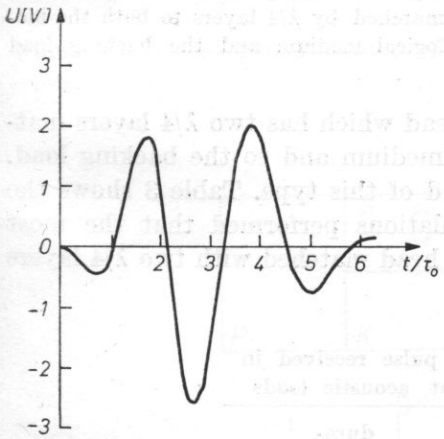

Fig. 8. The shape of voltage received for a transducer ideally loaded at the back, i.e. $z_0 = z_A$

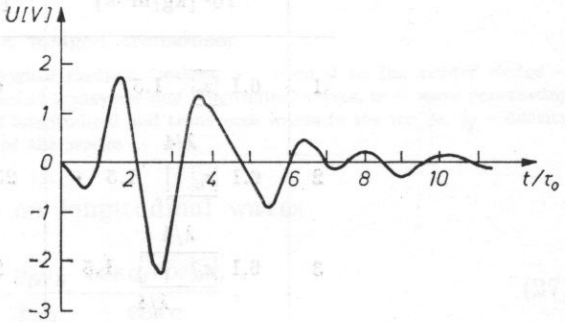

Fig. 9. Matching of the back load by a $\lambda/4$ layer

reflections occurring at the faces of the layers affect the shape of the response.

A large broadening of the frequency band of the head is obtained by an increase in the back load [9]. Fig. 8a shows the calculation results for a transducer which is loaded at the back by an impedance equal to its own. Although the greatest shortening of the response duration was obtained, the sensitivity of the head decreased at the same time. The next step, therefore, was an analysis of the operation of the head matched by a $\lambda/4$ layer to the backing load (Fig. 9).

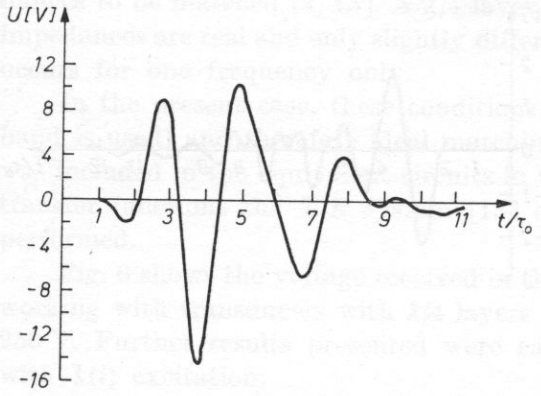

Fig. 10. Voltage received by a head matched by $\lambda/4$ layers to both the biological medium and the backing load

The result of these considerations is a head which has two $\lambda/4$ layers matching the transducer to both the biological medium and to the backing load. Fig. 10 shows the voltage received by a head of this type. Table 3 shows the results obtained. It follows from the calculations performed that the most suitable working conditions are assured by a head matched with two $\lambda/4$ layers (Table III, p. 6).

Table 3. Parameters of the pulse received in the *T-R* system for different acoustic loads

No.	acoustic load 10^6 [kg/m^2·s]	U_{max} [V]	duration t [s]	Fig.
1	6.1 $\boxed{z_0}$ 1.5	6.8	13.8 τ_0	4a
2	6.1 $\overset{\lambda/4}{\boxed{z_0}}$ 1.5	23.1	11.1 τ_0	6
3	6.1 $\overset{\lambda/4}{\boxed{z_0}}$ $\underset{\lambda/4}{}$ 1.5	2.2	8.1 τ_0	7
4	25.0 $\boxed{z_0}$ 1.5	2.6	5 τ_0	8
5	3.0 $\boxed{z_0}$ 1.5	2.4	10 τ_0	9
6	3.0 $\overset{\lambda/4\ \lambda/4}{\boxed{z_0}}$ 1.5	14.8	6.8 τ_0	10
7	6.1 $\boxed{z_0 \mid 33.0}$ 1.5	5.2	6.3 τ_0	13

$z_0 = 25 \cdot 10^6$ kg/m^{2}s

A wedged transducer

A completely different solution, with respect to the ones discussed previously, is the design of wedged transducer [2]; here also the improvement of the working conditions is achieved acoustically. Such a transducer consists of a conventional transducer which radiates an acoustic wave into the biological medium though a wedge made of material whose impedance is close to the acoustic impedance of the transducer (Fig. 11). The transfer function of the *T-R* system has the form

$$H_K(s) = E_{ll} H(s), \tag{26}$$

where E_{ll} is the transmittance of the echo.

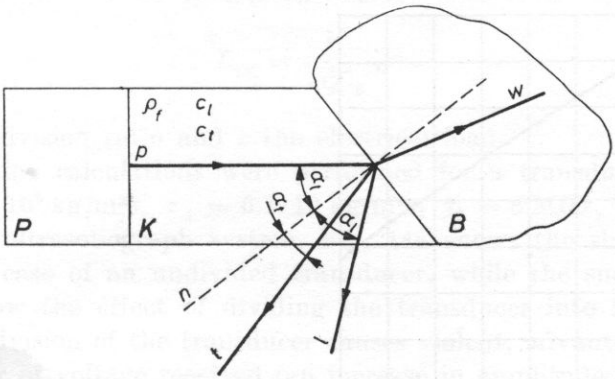

Fig. 11. A wedged transducer

P – transducer, *K* – matching wedge, *B* – biological medium (water), *n* – normal to the border wedge – water interface, *p* – the incident wave, *l*, *t* – reflected transverse and longitudinal waves, *w* – wave penetrating into the water (longitudinal), c_l, c_t – velocities of longitudinal and transverse waves in the wedge, ϱ_f – density of the wedge

For the *T-R* system working on longitudinal waves

$$E_{ll} = \frac{4}{N'} \frac{\varrho_B c_B}{\varrho_f c_l} \frac{\cos\alpha_l \cos^2\alpha_t}{\cos\alpha}, \tag{27}$$

where α is the angle between the direction of the incident wave and the normal to the plane of the edge, contiguous to the biological medium, α_t is the angle between the reflected transverse wave and the normal, and α_l is the angle

$$N' = \left(\frac{c_t}{c_l}\right)^2 \sin 2\alpha_l \sin 2\alpha_t + \cos^2 2\alpha_t + \frac{\varrho_B c_B \cos\alpha_l}{\varrho c_l \cos\alpha}. \tag{28}$$

Brass was chosen as the material for the wedge.

Attenuation in brass is very small and can be neglected in this case. The transmittance of the echo calculated for a transverse wave for the media: brass – water is given in Fig. 12. The lengths of one distances of the wedge are selected so that in the receiving transducer, the transverse wave does not fall on the plane of the transducer. For the wedged transducer designed, the shape of the voltage received in the T-R system of the ultrasonograph, for a $\mathbf{1}(t)$ excitation was calculated, and the results are shown in Fig. 13. The duration of the response was nearly halved, with only a slight decrease in the value of the maximum voltage, compared to the conventional transducer (cf. Fig. 4a).

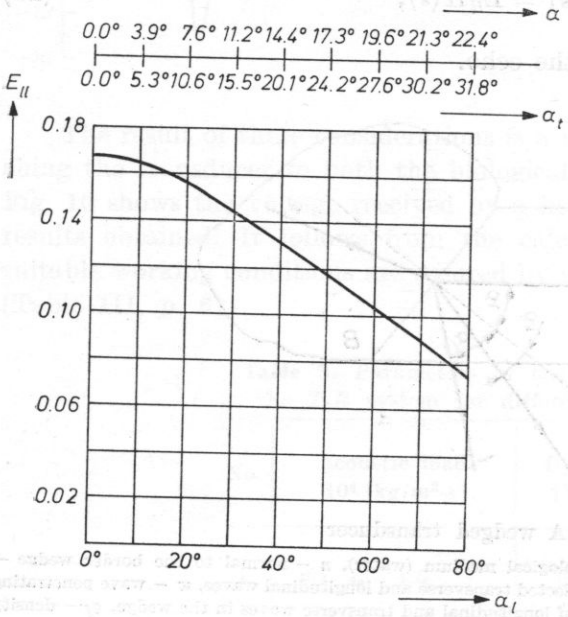

Fig. 12. Transmittance of the echo at the interface of brass – water

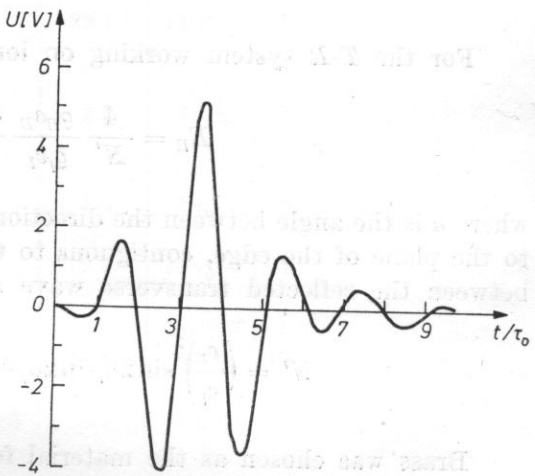

Fig. 13. The shape of voltage received in the T-R system working with wedge transducers

the parameters of the wedge: $z_k = 33 \cdot 10^6$ kg/m²s, the cone distances of the wedge: 55 mm and 77.5 mm ($\alpha_l = 40°$)

A divided transducer

One of the methods for matching the transducer to the electrical system at higher frequencies (the frequencies 8-12 MHz are used in ophtalmoscopy) is a division of the transducer and a serial connection of its parts. Thus an increase of the resistance of the transducer at resonance is achieved. The transmitting or receiving transfer function has the form

$$H' = \frac{N}{k}\frac{z}{z_0 A_0}[(m_A+1)e^{s\tau_0}-(m_A-1)e^{-s\tau_0}-2]\left\{\left[\left(1+\frac{z}{sL_{0K}}\right)k+\frac{zsC_0}{k}\right]\times\right.$$

$$\times[(m_A+1)(m_B+1)e^{s\tau_0}-(m_A-1)(m_B-1)e^{-s\tau_0}]-\frac{A}{s}\left(1+\frac{z}{sL_{0K}}\right)\times \qquad (29)$$

$$\left.\times k[(m_A+m_B+2)e^{s\tau_0}-(m_A+m_B-2)e^{-s\tau_0}-4\right\}^{-1}.$$

$$L_{0K}=\frac{k^2}{\omega_0^2 C_0},$$

where k is the division ratio and z the electrical load.

This time, the calculations were performed for a transducer with parameters $z_0 = 25\cdot10^6$ kg/m²s, $z_A = 6.1\cdot10$ kg/m²s, $f_0 = 8$ MHz, $C_0 = 2930$ pF; working in the ultrasonograph system. Fig. 14a shows the shape of voltage received in the case of an undivided transducer, while the successive results (Fig. 14b-d) show the effect of dividing the transducer into 2, 3, 4, 5 parts.

An initial division of the transducer causes violent, advantageous changes in the behaviour of voltage received (an increase in amplitude and a decrease in duration). There is a certain optimum division ratio, k, which assures best matching, beyond which further division of the transducer can cause distortions of amplitude and phase to occur in the response (see Table 4). In a specific system, the division cannot be arbitrary, but such as assures a matching of resistance of the transducer and the electrical system at the resonanse frequency.

Table 4. Parameters of the pulse received in the *T-R* system in the case of a divided transducer

No.		maximum voltage received U_{max} [V]	duration t [s]	Fig.	Remarks
1	transducer undivided	2.03	21.7 τ_0	14a	
2	2	9.84	15.4 τ_0	14b	
3	3	19.1	14.7 τ_0	14c	
4	4	23.4	11.6 τ_0	14d	occurrence
5	5	23.5	9.7 τ_0	14e	of distortions

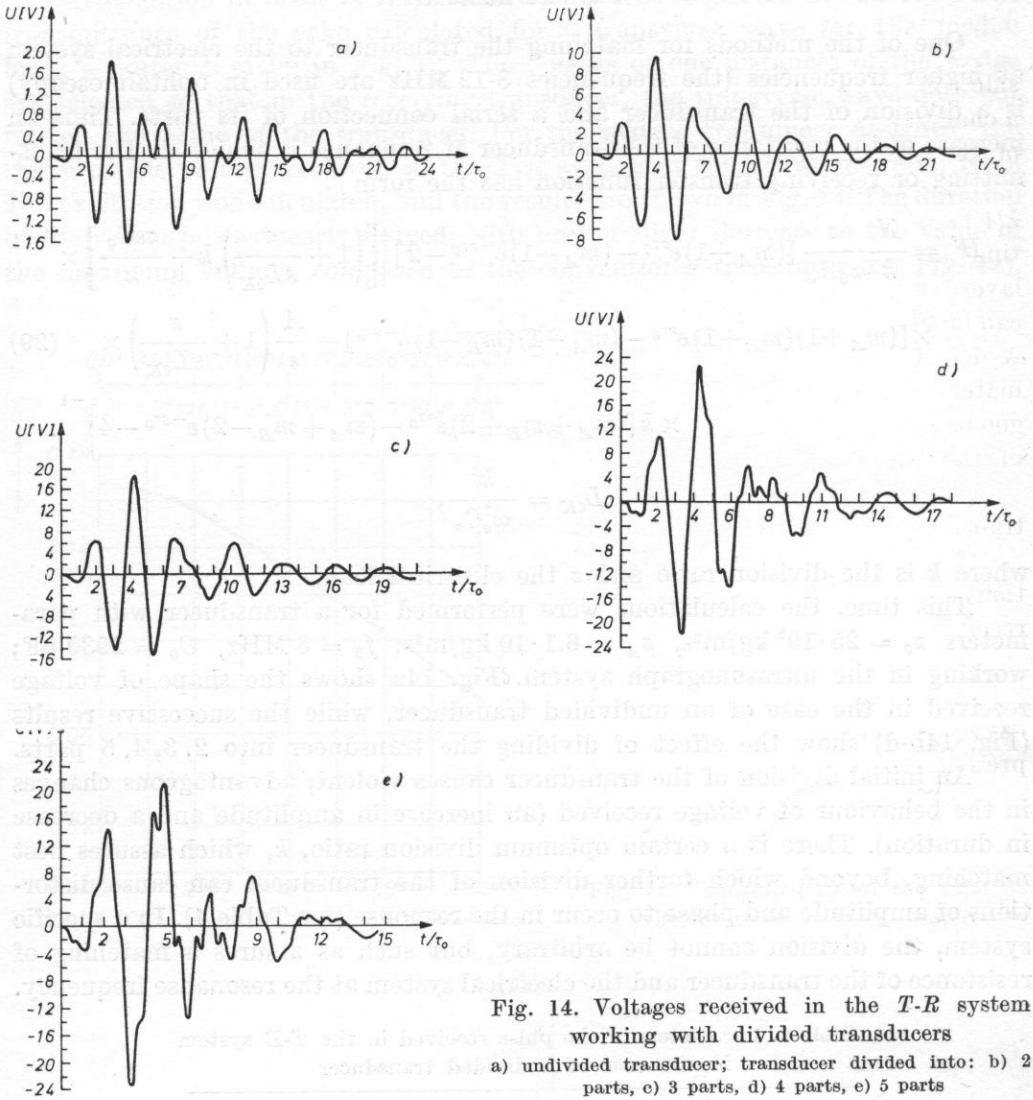

Fig. 14. Voltages received in the T-R system working with divided transducers

a) undivided transducer; transducer divided into: b) 2 parts, c) 3 parts, d) 4 parts, e) 5 parts

Conclusions

The method presented numerical calculation, using the FFT and circuit theory, appears to be relevant for the analysis of ultrasonic heads for different present combinations of parameters of the transducer and the T-R systems. Using the method described, a certain number of different desing solutions of heads were analyzed. From the results a number of conclusions can be formulated.

The multiple reflections occurring at both faces of the transducer have a decisive effect on the responses generated by and received by the head.

The selection of a suitable shape of electrical excitation on the transmitting side can improve the amplitude conditions of the whole T-R system. However, a change in the output impedance of the transducer not only changes the values of the maximum voltage received, but also its duration, in a broad range.

A matching of the transducer to the biological medium with just one $\lambda/4$ layer only slightly decreases the duration of the response, but at the same time increases the maximum value of voltage received. The use of two $\lambda/4$ layers advantageously decreases the duration of the pulse. Such a solution can be used particularly where we are interested in the early part of the response. A decrease in response duration can be achieved by increasing the backing matching directly, or by matching the transducer to it with a $\lambda/4$ layer. Fairly good results are obtained for a head working with two $\lambda/4$ layers on both sides of the transducer.

At higher frequencies, fairly good results can be obtained using a divided transducer.

The use of a wedged transducer considerably improves the working conditions, compared to a conventional transducer, decreasing the duration of signal received, while preserving almost the same sensitivity of the head.

Acknowledgement. I wish to express my gratitude to Prof. Dr. L. FILIPCZYŃSKI for all his valuable remarks and instructions, in the course of the present work.

References

[1] N. AHMED, R. RAO, *Orthogonal transforms for digital processing*, Springer-Verlag, Berlin 1975.

[2] G. A. ALPHONSE, *The wedged transducer: an improved transducer design for broad band characteristic and low insertion loss*, 1st Meeting of the World Federation for Ultrasound in Medicine and Biology, San Francisco, California, August 1-2 (1976).

[3] R. BRACEWELL, *The Fourier transform and its applications*, McGraw Hill, New York 1965.

[4] F. C. CRAWFORD, *Waves*, McGraw-Hill Book Company, New York 1965.

[5] W. J. DOMARKAS, R-I. J. KAŻYS, *Kontrolno-izmieritielnyje piezoelektriczeskije prieobrazowatieli*, "Mintis", Vilnius 1975.

[6] L. FILIPCZYŃSKI, *Transient equivalent circuit and negative capacitance of a piezoelectric transducer performing thickness vibrations*, Journal of Technical Physics, **16**, 2, 121-135 (1975).

[7] L. FILIPCZYŃSKI, D. KOMITOWSKI, G. ŁYPACEWICZ, B. ROŚCISZEWSKA, J. SAŁKOWSKI, *Ultrasonograph U0-3 for visualization of eye structures and its clinical uses*, Archiwum Akustyki, 8, 3, 265-282 (1973).

[8] Ch. KASAI, K. OKUYAMA, Y. KIKUCHI, *Transient response analysis of piezoelectric transducers using reflection and transmission coefficient at their surface*, Electronics and Communications in Japan, **56-A**, 3 (1973).

[9] C. KOSSOFF, *The effect of backing and matching on the performance of piezoelectric transducers*, IEEE Trans. **SU-13**, 1, 20-31 (1966).
[10] I. KRAUTKRÄMER, H. KRAUTKRÄMER, *Ultrasonic testing of materials*, Springer-Verlag, New York Inc., 1969.
[11] W. P. MASON, *Physical acoustics*, vol. I, part A, Academic Press, New York 1964.
[12] A. MARKIEWICZ, G. ŁYPACEWICZ, *The use of layers in matching ultrasonic probes to biological structures*, Proc. XXI Seminar on Acoustics, Rzeszów, 139-141 (1974).
[13] A. MARKIEWICZ, *Analysis of the effect of a $\lambda/4$ layer on the transient operation of a transducer*, Proc. XXII Open Seminar on Acoustics, Wrocław-Świeradów, 529-533 (1975).
[14] A. MARKIEWICZ, *Transient performance of piezoelectric transducer for medical diagnostics*. Proc. of FASE 78, II-56, 317-320, 1978.
[15] J. OSIOWSKI, *Theory of circuits*, WNT, Warszawa 1971.

Received on April 30, 1979; revised version on January 4, 1980.

Appendix

In the numerical elaboration of the analytical method, the following relations [1, 3] were used.

The continuous Fourier transform was defined in the following manner:

$$H(f) = \int_{-\infty}^{\infty} h(t) e^{-j2\pi ft} dt,$$

$$h(t) = \int_{-\infty}^{\infty} H(f) e^{j2\pi ft} dt,$$

$$h(t) \rightleftarrows H(f).$$

The principles of discrete representation of the function and its transform are formulated by the sampling function. In the time domain it has the form

$$\bigwedge_{f>f_c} H(f) = 0 \Rightarrow \hat{h}(t) = h(nT) \sum_{n=-\infty}^{\infty} \delta(t-nT) \wedge T = \frac{1}{2f_c},$$

where $\hat{h}(t)$ is a discrete function defining a continuous function $h(t)$, n is the number of samples, $\delta(t)$ is the Dirac function. However, in the frequency domain it is defined by the formula

$$\bigwedge_{t>T_c} h(t) = 0 \Rightarrow \hat{H}(f) = H\left(\frac{n}{2T_c}\right) \sum_{n=-\infty}^{\infty} \delta\left(f - \frac{n}{2T_c}\right)$$

and where $\hat{H}(f)$ is a discrete function defining a continuous function $H(f)$.

Discrete Fourier transform is defined by the following relations.

If $g(kT)$ is a sampled periodic function,

$$g(kT) = g[(rN+k)T], \quad r = 0, \pm 1, \pm 2, \ldots,$$

then discrete Fourier transformation is given by

$$G\left(\frac{n}{NT}\right) = \sum_{k=0}^{N-1} g(kT) e^{-j2\pi nk/N}, \quad n = 0, +1, +2, \ldots$$

with $G(n/NT)$ also being a periodic function:

$$G\left(\frac{n}{NT}\right) = G\left[\frac{(rN+n)}{NT}\right], \quad r = 0, \pm 1, \pm 2, \ldots$$

The inverse discrete Fourier transform has the form:

$$g(kT) = \sum_{n=0}^{N-1} G\left(\frac{n}{NT}\right) e^{j2\pi nk/N}, \quad k = 0, +1, +2, \ldots,$$

$$g(kT) \rightleftarrows G\left(\frac{n}{NT}\right).$$

If the discrete function $\hat{h}(t)$ approximates a continuous function $h(t)$, defined in the range $t \in \langle 0, L)$, then both continuous and discrete functions agree, with an exactness of a constant and

$$\hat{H}(nf_0) = LH\left(\frac{n}{NT}\right),$$

where H is the discrete Fourier transform, and $\hat{H}$ the discrete function approximating a continuous Fourier transform.

ARCHIVES OF ACOUSTICS
5, 3, 221-234 (1980)

ACOUSTIC PROPERTIES OF SELECTED LIQUIDS OVER THE ULTRA- AND HYPERSONIC RANGES

MIKOŁAJ ŁABOWSKI

Acoustics Department, UAM (60-769 Poznań, ul. Matejki 48/49)

The paper presents the results of the investigation of the ultra- and hypersonic properties of some selected liquids. It also analyses the temperature variation of the ratio $I_c/2I_{MB}$ in the fine structure of the Rayleigh line of scattered light. On the basis of the results of the experimental investigation it is shown that the following relaxation processes occur in the liquids investigated: rotational isomerism in *n*-hexane and iso-octane; structural relaxation in isobutyric acid and vibrational relaxation in *n*-heptane. It has been observed that no acoustic dispersion occurs in nitroethane below a frequency of ~4 GHz.

1. Introduction

Numerous association processes and the formation of complexes by hydrogen bonds or other weak chemical interactions, the rotation of isomers, and also the excitation and inactivation of intramolecular vibrations, occur in the liquid phase with characteristic times of the order of 10^{-6} to 10^{-12} s [1]. Such fast reactions have recently been successfully investigated, using acoustic spectroscopy methods which give information on the dispersion of velocity and absorption of ultra- and hypersonic waves propagating in liquid media. These are relaxation methods.

The condition for an acoustic method to be used in the investigation of the relaxation process mechanisms in liquid media is that the acoustic waves used in the investigations should have periods T close to the relaxation time, τ, of the process investigated. Thus the investigation of the nature of different relaxation processes having different relaxation times, should be performed over a wide frequency range.

The information obtained on a given relaxation process becomes the fuller, the broader the frequency spectrum of the ultrasonic waves used in the investigations becomes.

Very often only one normal reaction can be observed to occur in a system, and the spectrum of acoustic relaxation times is reduced to one value of τ [1]

$$\frac{\alpha}{f^2} = \frac{A}{1+(\omega\tau)} + B \tag{1}$$

and

$$\varepsilon = \frac{Av_0}{2\pi\tau} \tag{2}$$

where A is a parameter depending on the equilibrium characteristics.

The constants A and B are determined from the experimental shape of the dispersion curve, expressing the dependence of the quantity α/f^2 on $\log f$.

The following method is usually used for determination of the value of the quantities A, B, the relaxation time τ and the relaxation force ε. Using the quantity α/f^2, we check if for some frequencies in the dispersion range the frequency dependence of the quantity α/f^2 is, within the errors of measurement and calculation, described by expression (1). The values of A, B, and τ are then determined. Using the values found for A, B, τ and ε, the values of the relaxation force ε is calculated from formula (2).

The quantities A, B, τ, and ε are characteristic of relaxation processes occurring in liquids. These processes include for example: vibrational relaxation, structural relaxation, and rotational isomerism.

By investigation of the temperature dependence of the quantities A, ε, η_v/η_s, it is possible to identify the type of process involved [1], since these quantities decrease as temperature increases in the case of rotational isomerism, and increase in the case of vibrational relaxation. In the case of structural relaxation, the quantities A and ε decrease, while η_v/η_s is practically independent of temperature.

The velocity and absorption coefficient of the acoustic waves were measured at three independent measuring positions at frequencies from 20 MHz to 150 MHz, and 300 MHz to 1000 MHz, using suitable pulse methods involving resonance and non-resonance excitation of piezoelectric transducers, and also at hypersonic frequencies, from the displacement and half power width of the Mandelshtam-Brillouin components in the fine structure of the Rayleigh lines scattered light.

The propagation velocity and absorption coefficient of hypersonic waves, and the $I_c/2I_{MB}$ ratio were determined at different temperatures from photoelectrical recordings of the fine structure of Rayleigh light scattering. The liquids used in the investigation were additionally cleaned chemically and distilled. The degree of purity was controlled through measurements of refractive index and density.

An exact description of the measuring apparatus and methodology is given elsewhere [2, 18].

The values of α_{kl}/f^2, the coefficient of volume viscosity, and the coefficient of adiabatic compressibility were calculated from the formulae:

$$\frac{\alpha_{kl}}{f^2} = \frac{8}{3}\frac{\pi^2\eta_s}{\varrho v_0^3}, \tag{3}$$

$$\eta_v = \frac{A\varrho v_0^3}{2\pi^2}, \tag{4}$$

$$\beta = \frac{1}{\varrho v^2}, \tag{5}$$

where η_s is the coefficient of shear viscosity, and ϱ is density. A maximum absorption on the wavelength, $\mu_{\max}$, at a frequency $f = f_m$ was found from the expression

$$\mu_{\max} = \frac{Avf_m}{2}. \tag{6}$$

The ratio of the total intensity of the central line to the total intensity of the Mandelshtam-Brillouin lines was determined for all the media investigated according to the formula (given in [3])

$$\left(\frac{I_c}{2I_{MB}}\right)_{\text{total}} = \left(\frac{I_c}{2I_{MB}}\right)_{\max}\frac{\delta\nu_c}{\delta\nu_{MB}}, \tag{7}$$

where $\delta\nu$ and $\delta\nu_{MB}$ are the half power widths of the central and lateral components.

The results are presented below of the acoustic investigation of the following selected pure liquids: isobutyric acid, *n*-heptane, *n*-hexane, iso-octane, nitroethane in both ultrasonic and hypersonic ranges.

The selection of the different objects for the investigation was caused, among other things, by the fact that they are components of the critical mixtures [19]. In addition, an attempt was made to show that the thermodynamics of irreversible processes, as developed by MASON [1], provides a sufficiently universal method and which can be used for the explanation of the molecular mechanisms of reactions occurring in different liquids.

2. Measurement results and their interpretation

2.1. Isobutyric acid. The acoustic properties of isobutyric acid were investigated in both ultra- and hypersonic ranges. As an illustration, Fig. 1 shows the original recordings of the fine structure of the Rayleigh line of light scattered at an angle $\theta = 90°$ in isobutyric acid at selected temperatures. The values of $\Delta\nu, f, I_c/2I_{MB}$ are shown at the side of each recording, while the dependence of $I_c/2I_{MB}$ on temperature is plotted in Fig. 2.

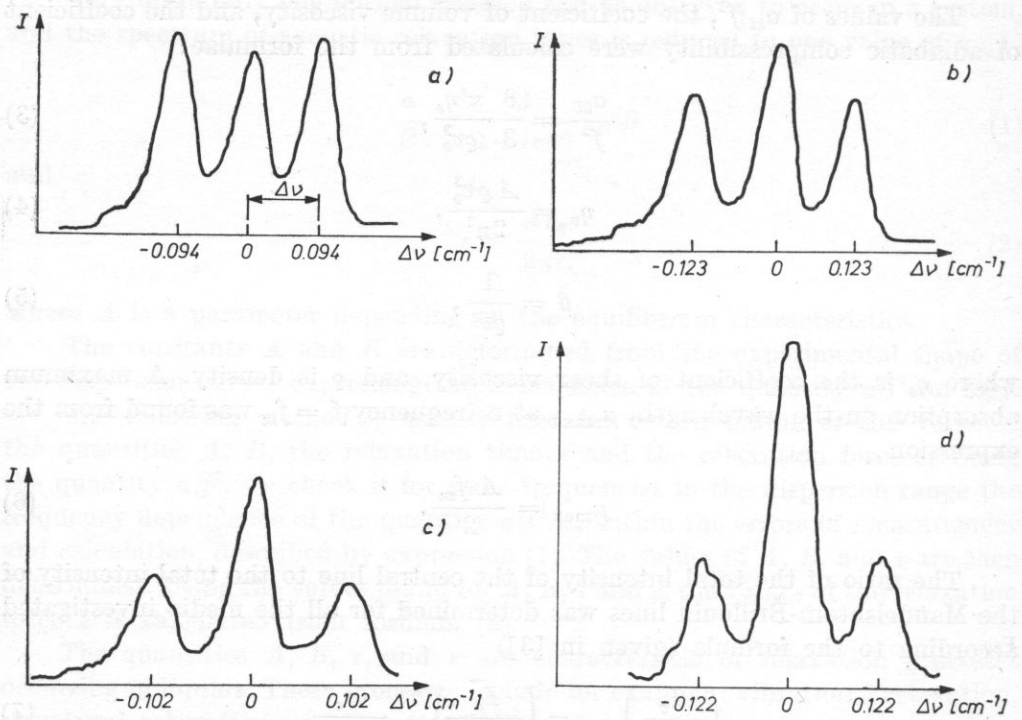

Fig. 1. Variation behaviour in the original recordings of the fine structure of the Rayleigh line of light scattered at an angle $\theta = 90°$ for isobutyric acid at different temperatures

a) $t = 75°C$, $\Delta\nu = 0.094\ cm^{-1}$, $f = 2.8GHz$, $I_c/2I_{MB} = 0.459$;
b) $t = 45°C$, $\Delta\nu = 0.123\ cm^{-1}$, $f = 3.69GHz$, $I_c/2I_{MB} = 0.686$;
c) $t = 25°C$, $\Delta\nu = 0.102\ cm^{-1}$, $f = 3.07GHz$, $I_c/2I_{MB} = 0.982$;
d) $t = 18°C$, $\Delta\nu = 0.122\ cm^{-1}$, $f = 3.68GHz$, $I_c/2I_{MB} = 1.220$.

The results obtained for the absorption coefficient of the ultrasonic waves of varying frequencies at temperatures of 10°, 20°, 30° and 40°C are shown graphically in Figs. 3 and 4.

It can be seen from Figs. 3 and 4 that acoustical relaxation occurs within the investigated region of frequencies and temperatures. It can also be seen from the character of the curves for the dependence of the quantity α/f^2 on $\log f$, that this is the second range of acoustic relaxation for isobutyric acid.

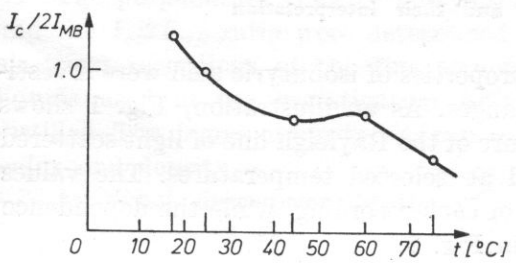

Fig. 2. Dependence of $I_c/2I_{MB}$ on temperature for isobutyric acid

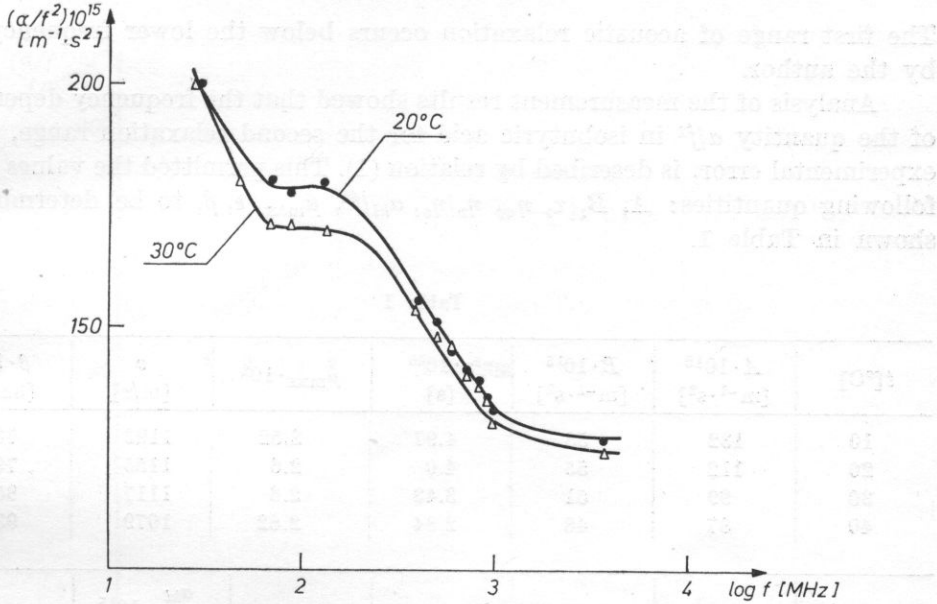

Fig. 3. Dependence of α/f^2 on log$f$ for isobutyric acid at temperatures of 20°C and 30°C

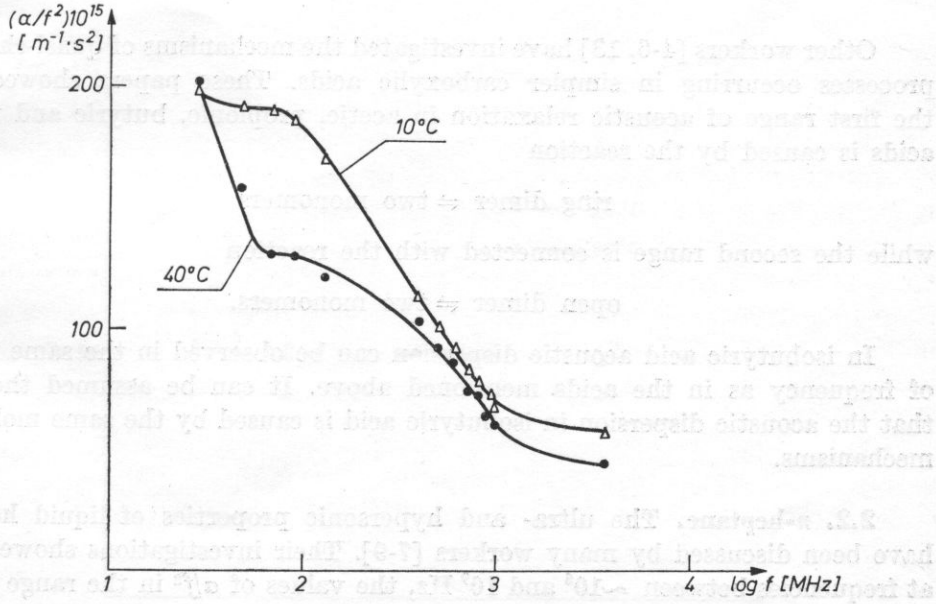

Fig. 4. Dependence of α/f^2 on log$f$ for isobutyric acid at temperatures of 10°C and 40°C

The first range of acoustic relaxation occurs below the lower frequency used by the author.

Analysis of the measurement results showed that the frequency dependence of the quantity α/f^2 in isobutyric acid for the second relaxation range, within experimental error, is described by relation (1). This permitted the values of the following quantities: A, B, τ, η_v, η_v/η_s, a_{kl}/f^2, μ_{max}, ε, β, to be determined as shown in Table 1.

Table 1

t[°C]	$A\cdot 10^{15}$ [m$^{-1}\cdot$s^2]	$B\cdot 10^{15}$ [m$^{-1}\cdot$s^2]	$\tau\cdot 10^{10}$ [s]	$\mu_{max}\cdot 10^2$	v [m/s]	$\beta\cdot 10^6$ [bar^{-1}]
10	132	58	4.97	2.52	1193	73.6
20	112	55	4.0	2.6	1155	79.5
30	99	51	3.43	2.6	1117	85.5
40	87	48	2.84	2.62	1079	93.0

t[°C]	$\varepsilon\cdot 10^2$	η_s [cP]	η_v [cP]	η_v/η_s	$\frac{a_{kl}}{f^2}\cdot 10^{15}$ [m$^{-1}\cdot$s^2]	ϱ [g/cm^3]
10	1.62	1.568	11	7	25.2	0.9592
20	1.66	1.318	8.35	6.5	23.8	0.9504
30	1.66	1.129	6.6	5.85	22.7	0.9414
40	1.67	0.98	5.2	5.3	21.9	0.9325

Other workers [4-6, 13] have investigated the mechanisms of quasi-chemical processes occurring in simpler carboxylic acids. These papers showed that the first range of acoustic relaxation in acetic, propionic, butyric and valeric acids is caused by the reaction

$$\text{ring dimer} \rightleftharpoons \text{two monomers}$$

while the second range is connected with the reaction

$$\text{open dimer} \rightleftharpoons \text{two monomers.}$$

In isobutyric acid acoustic dispersion can be observed in the same ranges of frequency as in the acids mentioned above. It can be assumed therefore that the acoustic dispersion in isobutyric acid is caused by the same molecular mechanisms.

2.2. *n*-heptane. The ultra- and hypersonic properties of liquid heptane have been discussed by many workers [7-9]. Their investigations showed that at frequencies between $\sim 10^6$ and 10^9 Hz, the values of α/f^2 in the range of the measurement error do not depend, within experimental error, on the frequency, and exceed the values of the quantity a_{kl}/f^2 by more than a factor of five.

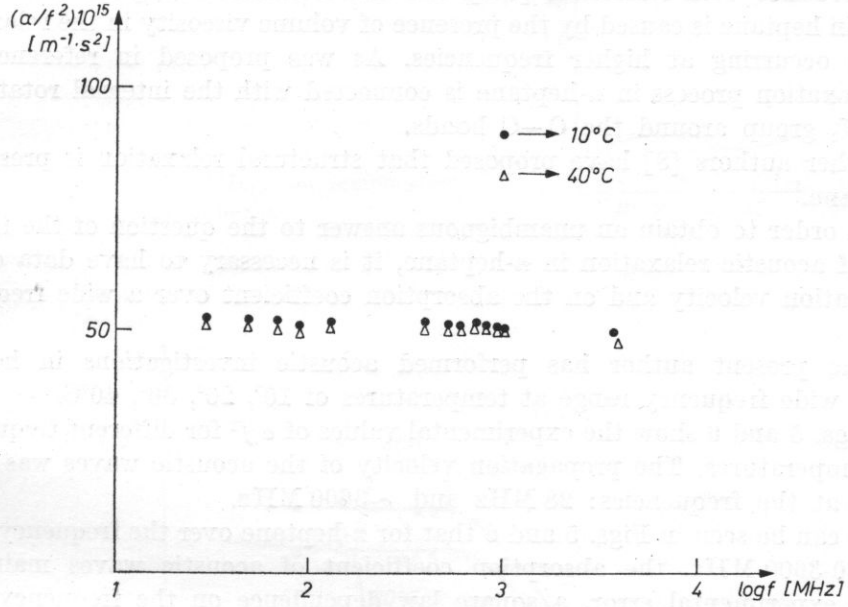

Fig. 5. Dependence of α/f^2 on log$f$ for n-heptane at temperatures of 10°C and 40°C

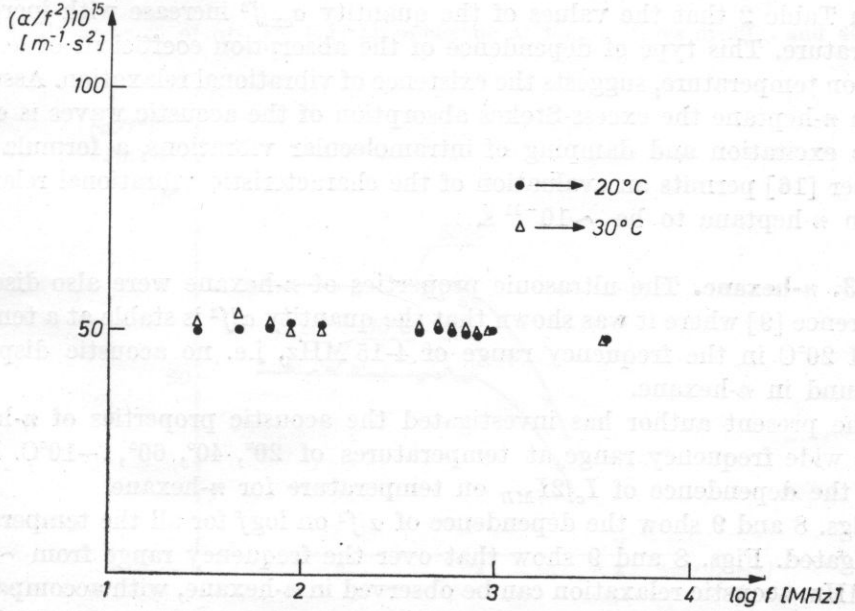

Fig. 6. Dependence of α/f^2 on log$f$ for n-heptane at temperatures of 20°C and 30°C

In accordance with references [7-9], the excess-Stokes absorption of acoustic waves in heptane is caused by the presence of volume viscosity in the relaxation process occurring at higher frequencies. As was proposed in reference [7], the relaxation process in *n*-heptane is connected with the internal rotation of the CH_3 group around the C—C bonds.

Other authors [8] have proposed that structural relaxation is present in *n*-heptane.

In order to obtain an unambiguous answer to the question of the mechanism of acoustic relaxation in *n*-heptane, it is necessary to have data on the propagation velocity and on the absorption coefficient over a wide frequency range.

The present author has performed acoustic investigations in heptane over a wide frequency range at temperatures of 10°, 20°, 30°, 40°C.

Figs. 5 and 6 show the experimental values of α/f^2 for different frequencies and temperatures. The propagation velocity of the acoustic waves was determined at the frequencies: 28 MHz and ~3600 MHz.

It can be seen in Figs. 5 and 6 that for *n*-heptane over the frequency range of ~20-3600 MHz, the absorption coefficient of acoustic waves maintains, within experimental error, a square law dependence on the frequency.

The experimental values of α_{ex}/f^2, v_0, α_{kl}/f^2, η_s, η_v, η_v/η_s, α_{ex}/α_{kl}, and also the values of C_p, C_v and the total specific heat of vibration C^*_{opt}, are shown in Table 2.

The values of C_{opt} are found from the data on the normal frequencies of vibration of the molecules, using the Planck-Einstein formula [1]. It can be seen in Table 2 that the values of the quantity α_{ex}/f^2 increase with increasing temperature. This type of dependence of the absorption coefficient of acoustic waves on temperature, suggests the existence of vibrational relaxation. Assuming that in *n*-heptane the excess-Stokes absorption of the acoustic waves is caused by the excitation and damping of intramolecular vibrations, a formula given in paper [16] permits an evaluation of the characteristic vibrational relaxation time in *n*-heptane to be $\sim 10^{-11}$ s.

2.3. *n*-hexane. The ultrasonic properties of *n*-hexane were also discussed in reference [9] where it was shown that the quantity α/f^2 is stable at a temperature of 20°C in the frequency range of 4-15 MHz, i.e. no acoustic dispersion was found in *n*-hexane.

The present author has investigated the acoustic properties of *n*-hexane over a wide frequency range at temperatures of 20°, 40°, 60°, —10°C. Fig. 7 shows the dependence of $I_c/2I_{MB}$ on temperature for *n*-hexane.

Figs. 8 and 9 show the dependence of α/f^2 on log$f$ for all the temperatures investigated. Figs. 8 and 9 show that over the frequency range from ~20 to 3500 MHz, acoustic relaxation can be observed in *n*-hexane, with accompanying weak dispersion of the wave propagation velocity: ~0.012. The value of

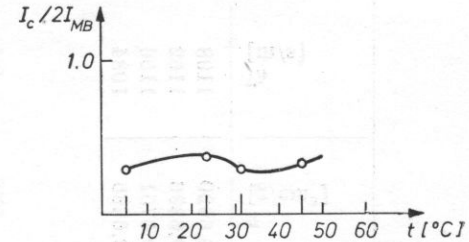

Fig. 7. Dependence of $I_c/2I_{MB}$ on temperature for n-hexane

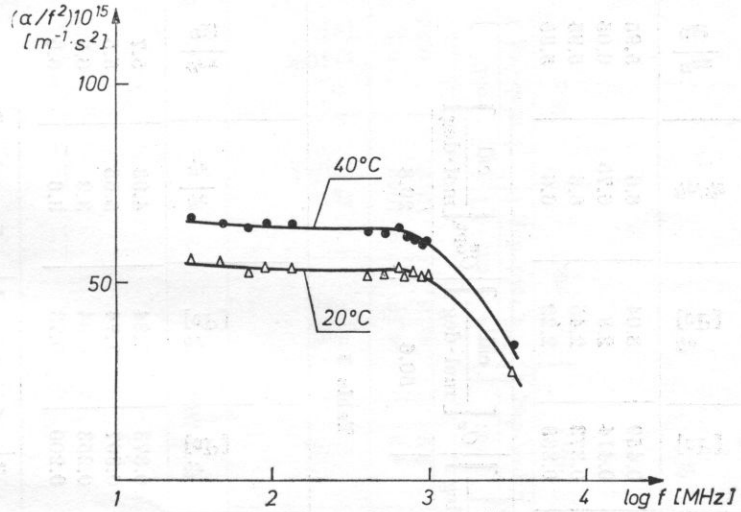

Fig. 8. Dependence of a/f^2 on log$f$ for n-hexane at temperatures of 20°C and 40°C

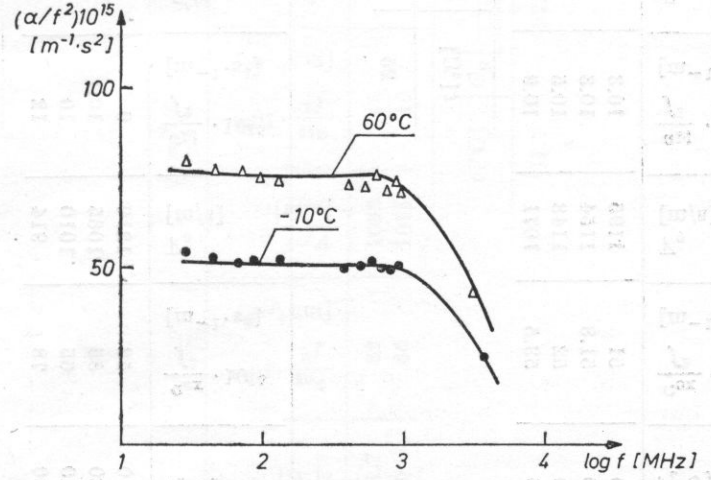

Fig. 9. Dependence of a/f^2 on log$f$ for n-hexane at temperatures of 60°C and −10°C

Table 2

t [°C]	$\frac{a_{ex}}{f^2}\cdot 10^{15}$ [$m^{-1}\cdot s^2$]	V_0 [m/s]	$\frac{a_{kl}}{f^2}\cdot 10^{15}$ [$m^{-1}\cdot s^2$]	$\frac{a}{f^2}\cdot 10^{15}$ [$m^{-1}\cdot s^2$]	η_s [cP]	η_v [cP]	η_v/η_s	$\frac{a_{ex}}{a_{kl}}$	ϱ [g/cm^3]	v_h [m/s]
10	51	1195	10.3	40.7	0.459	3.04	6.6	5.95	0.6920	1198
20	51.8	1154	10.3	41.5	0.414	2.8	6.75	6.05	0.6836	1162
30	52	1148	10.5	41.5	0.373	2.45	6.6	5.95	0.6751	1156
40	53.5	1071	10.9	42.6	0.338	2.22	6.6	5.95	0.6665	1084

t [°C]	$C_p\left[\frac{\text{cal}}{\text{mol}\cdot\text{deg}}\right]$	$C_v\left[\frac{\text{cal}}{\text{mol}\cdot\text{deg}}\right]$	$C^*_{opt}\left[\frac{\text{cal}}{\text{mol}\cdot\text{deg}}\right]$
25	53.4	50.6	29.8

Table 3

t [°C]	$\frac{a_{ex}}{f^2}\cdot 10^{15}$ [$m^{-1}\cdot s^2$]	V_0 [m/s]	$\frac{a_{kl}}{f^2}\cdot 10^{15}$ [$m^{-1}\cdot s^2$]	$\frac{a'}{f^2}\cdot 10^{15}$ [$m^{-1}\cdot s^2$]	η_s [cP]	η_v [cP]	$\frac{\eta_v}{\eta_s}$	$\frac{a_{ex}}{a_{kl}}$	v_h [m/s]	$\tau\cdot 10^{10}$ [s]
−10	52	1210	9	43	0.373	1.84	4.93	5.7	1220	0.81
20	55	1065	10.1	44.9	0.307	1.74	5.65	5.5	1078	0.80
40	65	1010	10	55	0.253	0.84	3.3	6.5	1009	0.76
60	78	914	12	66	0.200	0.73	3.6	6.5	919	0.69

t [°C]	$C_p\left[\frac{\text{cal}}{\text{mol}\cdot\text{deg}}\right]$	$C_v\left[\frac{\text{cal}}{\text{mol}\cdot\text{deg}}\right]$	$C^*\left[\frac{\text{cal}}{\text{mol}\cdot\text{deg}}\right]$
20	46.3	35.8	24.6

Table 4

t[°C]	$\frac{a_{ex}}{f^2}\cdot 10^{15}$ [$m^{-1}\cdot s^2$]	V_0 [m/s]	$\frac{a_{kl}}{f^2}\cdot 10^{15}$ [$m^{-1}\cdot s^2$]	$\frac{a'}{f^2}\cdot 10^{15}$ [$m^{-1}\cdot s^2$]	η_v/η_s	$\frac{a_{ex}}{a_{kl}}$	v_h [m/s]	$\tau\cdot 10^{10}$ [s]	$\mu_{max}\cdot 10^2$	$\varepsilon\cdot 10^2$
1.7	62	1053	15	47	4.3	4.13	1059	0.3	10.7	6.9
40	66	1014	16	50	3.9	4.15	1019	0.26	10.3	6.4

t[°C]	$C_p\left[\frac{\text{cal}}{\text{mol}\cdot\text{deg}}\right]$	$C_v\left[\frac{\text{cal}}{\text{mol}\cdot\text{deg}}\right]$	$C_p^0\left[\frac{\text{cal}}{\text{mol}\cdot\text{deg}}\right]$	$C^*\left[\frac{\text{cal}}{\text{mol}\cdot\text{deg}}\right]$
31.7	57.6	45.9	46.7	38.2

$(\Delta v/v)_{\text{theor}}$ ~0.0101, which agrees with the experimental value, within experimental error. Thus the relaxation process observed can be described with one value of τ.

The acoustic parameters are given in Table 3.

According to previous investigations [10], associated complexes do not exist in *n*-hexane at the expense of hydrogen bonds.

In the liquid and gaseous states, *n*-hexane takes the form of a mixture of rotational isomers. Answering the question as to which of the possible rotational isomers are actually present in the medium investigated, involves considerable experimental difficulties.

Calculations made using the Herzfeld formula given in reference [17] showed that the vibrational relaxation in *n*-hexane has a time of $\sim 0.6 \cdot 10^{-11}$ s, i.e. it is shorter by an order of magnitude than the experimentally found value of $\tau = 0.8 \cdot 10^{-10}$ s. Thus the relaxation process observed in *n*-hexane in the frequency range of $\sim 10^7$-$3.5 \cdot 10^9$ Hz and in the temperature range investigated is, in all probability, caused by rotational-isomeric changes in the molecules of *n*-hexane.

Using the values of τ, the height of the energetic barrier between the rotational configurations was evaluated as ~3.5 kcal/mol.

2.4. Iso-octane. The acoustic properties of iso-octane were investigated over the frequency range from ~20-3400 MHz by pulse and optical methods. Fig. 10 shows the dependence of $I_c/2I_{MB}$ on temperature.

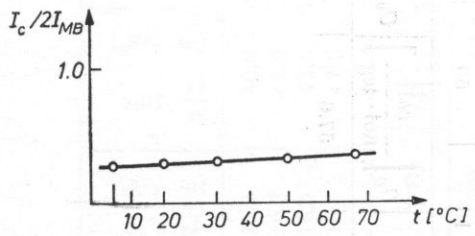

Fig. 10. Dependence of $I_c/2I_{MB}$ on temperature for iso-octane

Data on the amplitude absorption coefficient of acoustic waves at different frequencies and two temperatures are shown in Fig. 11 where the dependence of α/f^2 on log$f$ is presented graphically.

Fig. 11 shows that in iso-octane over the frequency range of ~20-1000 MHz, α/f^2 is, within experimental error, independent of the frequency, being $\sim 62 \cdot 10^{-17}$ cm^{-1} s^2. For a hypersonic frequency of ~3.4 GHz α/f^2 decreases to $48 \cdot 10^{-17}$ cm^{-1} s^2, which suggests that in the frequency range of ~20 MHz-3.4 GHz a relaxation process with a relaxation time of $\sim 0.4 \cdot 10^{-10}$ s occurs in iso-octane. Using the value of $\tau = 0.4 \cdot 10^{-10}$ s, $(\Delta v/v)_{\text{theor}}$ was calculated. The result, $(\Delta v/v)_{\text{theor}} = 0.3\%$, agrees with the observed value $(\Delta v/v)_{\text{ex}} = 0.2\%$. This agreement of theoretical and experimental values of $\Delta v/v$ suggets that

the acoustic relaxation observed in iso-octane over the investigated frequency range is characterized by one value of τ. All the parameters defined are shown in Table 4.

According to earlier investigations [11], associated complexes with vibrational relaxations occurring at frequencies higher than $\sim 10^{10}$ Hz do not occur in liquid iso-octane.

It can be seen in Table 4 that the value of η_v/η_s is not the same at both temperatures, since it is lower for the higher temperature. This permits the assumption that in iso-octane, as in other paraffins [12], the acoustic dispersion is connected with rotational-isomeric transformations of the iso-octane molecules.

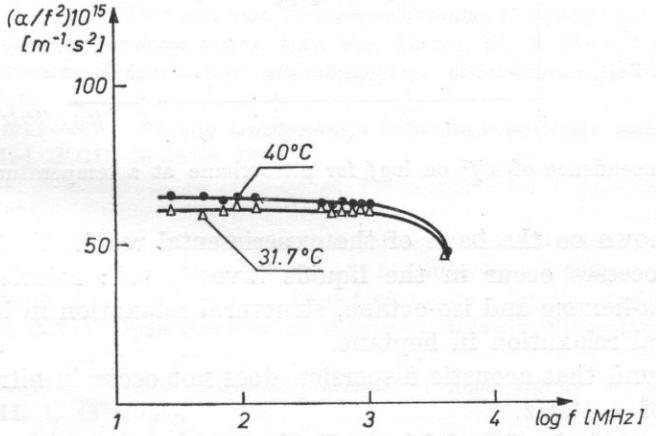

Fig. 11. Dependence of α/f^2 on $\log f$ for iso-octane

Then, using the experimentally found value of τ, the height of the energetic barrier between the two configurations can be evaluated as $\sim$3.3 kcal/mol, which agrees with the values obtained by PIERCY for other paraffins [12].

On the other hand, it is interesting to evaluate the vibrational relaxation time.

The values of C_p, C_v, C_p^0, C_{opt}^* are shown in Table 4. The vibrational relaxation time τ, obtained for iso-octane was found to be $\sim 0.6 \cdot 10^{-11}$ s, i.e. shorter by an order of magnitude than the experimental value of $\sim 0.4 \cdot 10^{-10}$ s.

This circumstance confirms the thesis that acoustic relaxation in iso-octane is caused by rotational-isomeric transformations of the iso-octane molecules.

2.5. Nitroethane. The ultra- and hypersonic investigations showed that acoustic dispersion does not occur in pure nitroethane below a frequency of $\sim$4 GHz. Fig. 12 shows graphically the dependence of α/f^2 on $\log f$ over the whole range

of frequencies investigated, at a temperature $t = 31.7°C$. It can be seen that within experimental error, the absorption coefficient of the acoustic waves is proportional to the square of the frequency, and the values of α/f^2 are relatively low. Fig. 13 shows the dependence of $I_c/2I_{MB}$ on temperature.

The values of A, B, τ, η_v, η_v/η_s, ε, β, μ_{max}, v_0, v_n, α_{ex}/f^2, α_{kl}/f^2, $\Delta\nu$, $\delta\nu_{MB}$, $I_c/2I_{MB}$, have been determined for all the liquids investigated.

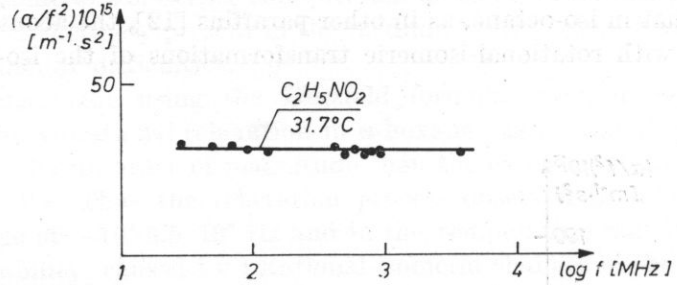

Fig. 12. Dependence of α/f^2 on $\log f$ for nitroethane at a temperature of 31.7°C

It was shown on the basis of the experimental results that the following relaxation processes occur in the liquids investigated: rotational isomerism relaxation in *n*-hexane and iso-octane, structural relaxation in isobutyric acid, and vibrational relaxation in heptane.

It was found that acoustic dispersion does not occur in nitroethane below a frequency of ~4GHz.

Recordings of the Mandelshtam-Brillouin spectra and measurements of the absorption coefficient and propagation velocity of ultrasonic waves were made in Prof. M. I. SHAKHPARONOV's Solutions Laboratory, at the M. W. Lomonosov University in Moscow, in Dr. O. I. ZINOVYIEV's section, to whom the author wishes to express his gratitude.

The author wishes to thank Prof. Dr. hab. A. ŚLIWIŃSKI from Gdańsk University for numerous valuable discussions of the results obtained.

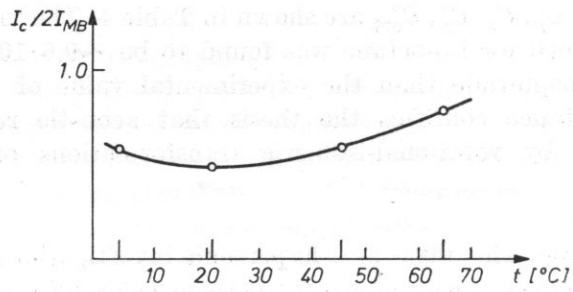

Fig. 13. Dependence of $I_c/2I_{MB}$ on temperature for nitroethane

References

[1] P. Mason, *Physical Acoustics II A*, New York–London 1965.

[2] M. Łabowski, *Ultra- and hypersonic properties of a critical mixture of nitroethane – iso-octane* (Archives of Acoustics, in press).

[3] I. Ł. Fabielinskij, *Molekularnoje rassiejanije swieta*, Izd. Nauka, Moskwa 1965.

[4] L. W. Łanszyna, M. I. Linina, P. K. Chabibullajew, *Wtoraja oblast relaksacyi w karbonowych kislotach*, Akust. Żurnał, **16**, 3, 413-418 (1970).

[5] A. V. Anantaraman, A. B. Walters, P. D. Edmonds, C. J. Pings, *Absorption of sound near the critical point of the nitrobenzene – iso-octane system*, J. Chem. Phys., **44**, 7, 2651-2658 (1966).

[6] I. Lamb, J. M. M. Pinkerton, *The absorption and dispersion of ultrasonic waves in acids*, Proc. Roy. Soc., **A199**, 114-129 (1949).

[7] J. E. Piercy, M. G. Seshagieri Rao, *Ultrasonic relaxation due to trans-gauche rotational isomers in the liquid normal paraffins*, J. Chem. Phys., **46**, 10, 3951-3959 (1967).

[8] G. P. Roszczyna, G. Ł. Gudimienko, *Issledowanije tonkoj struktury linii Releja w n-parafinach s pomoszczziu gazowego łazera*, Ukr. Fiz. Żurnał, **15**, 6, 888-892 (1970).

[9] W. F. Nozdriew, *Primienienije ultraakustiki w molekularnoj fizikie*, Izd. Nauka, Moskwa (1958).

[10] M. I. Szachparonow, *Mietody issledowanija tiepłowogo dwiżenija molekuł i strojenija żydkostiej*, Izd. MGU, Moskwa 1963.

[11] K. G. Plass, *Relaxationen in organischen Flüssigkeiten bei 1 GHz*, Acoustica, **19**, 4, 236-242 (1967).

[12] J. E. Piercy, *Ultrasonic relaxation and the barrier to internal rotation in 1,2 dichloro- and 1,2 dibromoethane*, J. Chem. Phys., **43**, 11, 4066-4071 (1965).

[13] A. Juszkiewicz, Z. Bortynowska, *Second ultrasonic relaxation region in acetic acid esthers*, Proc. XXIV Open Seminar on Acoustics, Gdańsk-Władysławowo 1977, 166-169.

[14] Z. Kleszczewski, *Thermal relaxation processes in some organic liquids*, Archives of Acoustics, **11**, 1, 43 (1976).

[15] P. Miecznik, *Ultrasonic and hypersonic investigations of vibrational relaxation in liquid thiofene*, Arch. Acoust. **13**, 4, 301-309 (1978).

[16] L. D. Landau, E. Tieller, *Sobranije trudow*, vol. 1, Izd. Nauka, Moskwa 1969.

[17] K. F. Herzfeld, T. A. Litowitz, *Absorption and dispersion of ultrasonic waves*, Academic Press Inc., New York 1959.

[18] O. I. Zinowiew, *Ustanowka dla izuczenija skorosti i pogłoszczenija zwuka w żydkostjach na czastotach ot 2 do 6-7 GHz*, Wiestn. MGU, Chimija, **2**, 166-170 (1975).

[19] M. Łabowski, *Acoustic wave absorption, measured in selected critical mixtures throughout a wide range of frequencies, in comparison with Fixman's theory*, Acoustics Letters, **2**, 130-136 (1979).

Received on May 12, 1979; revised version on December 18, 1979.

ARCHIVES OF ACOUSTICS
5, 3, 237-250 (1980)

MUTUAL ACOUSTIC IMPEDANCE OF CIRCULAR MEMBRANES AND PLATES WITH BESSEL AXIALLY-SYMMETRIC VIBRATION VELOCITY DISTRIBUTIONS

WITOLD RDZANEK

Theoretical Physics Department, Higher Pedagogical School
(65-069 Zielona Góra, Plac Słowiański 6)

In this paper the mutual impedance of circular membranes and circular plates clamped at the circumference is analyzed. It was assumed that a Bessel axially-symmetric vibration velocity distribution was predetermined on the surface of the sources, and that the sources were placed in a rigid planar baffle. The impedance was calculated by a method based on a Fourier representation of the acoustic pressure. In view of the axially-symmetric vibration velocity distribution, the acoustic pressure and the subsequent formulae for the mutual impedance are given in the Hankel representation. As a result, the mutual impedance can be expressed in the form of a single integral. Practically useful formulae are derived for specific cases. The results of the calculation are also shown graphically.

1. Introduction

Most of the planar acoustic sources that have a practical usefulness, are characterized by a nonuniform vibration velocity distribution. The Bessel vibration velocity distributions have a particular significance, since they are suitable for an exact description of the problem of the vibration of a membrane or of a circular plate clamped at the circumference.

The literature on the acoustic impedance of source with nonuniform vibration velocity distributions contains only a few items.

The problem of the mutual impedance of two elastic circular pistons vibrating in the flexural mode was investigated in 1964 by PORTER [5] and CHAN [1] in 1967. They assumed that the vibration velocity distribution was axially-symmetric and could be expressed by a power series in the radial variable.

The problem of the mutual impedance of two circular sources with nonuniform axially-symmetric vibration velocity distributions, namely: gaussian,

parabolic and Bessel distributions, was investigated by the author in papers [6-10] in the 1970's.

The problems presented in the present paper are connected with the mutual impedance of circular membranes and circular plates clamped at the circumference. It has been assumed in the calculation of the impedance that there is a Bessel axially-symmetric vibration velocity distribution on the surface of the sources, and that they are situated in ideal rigid planar baffles. The results of the calculations are presented graphically.

Notation

The numbers in parentheses denote the formulae giving definition or application of the symbol.

a – radius of the circle,
c – the wave velocity,
f – the vibration velocity distribution function,
$H_p^{(2)}$ – a cylindrical Hankel function of the second kind of the pth order,
$h_p^{(2)}$ – a spherical Hankel function of the second kind of the pth order (27),
i – $\sqrt{-1}$,
J_n – a cylindrical Bessel function of the nth order,
j_m – a spherical Bessel function of the mth order (24),
k – the wave number,
l_{12} – the distance between the centres of sources 1 and 2,
N_m – a cylindrical Neumann function of the mth order,
n_m – a spherical Neumann function of the mth order (26),
p_{12} – the acoustic pressure generated by source 1 acting on source 2 (10),
R – the distance between two points on the two sources,
r – the radial variable in a polar coordinate system,
t – time,
U – a characteristic function of the source (15),
v – the vibration velocity of points of the source,
v_0 – the vibration velocity of the central point on the surface of the source,
W – a characteristic function of the source for an axially-symmetric vibration velocity distribution (17),
Z_{11} – the mechanical self-impedance of one source,
Z_{12} – the mechanical mutual impedance of two sources (9),
θ_{12} – the normalised mutual resistance (11),
χ_{12} – the normalised mutual reactance (11),
ζ_{12} – the normalised mutual impedance (11),
ϱ – the density of the medium,
σ – the area of the source,
ω – the angular frequency.

2. Assumptions of the analysis

It is assumed that in an infinite ideal liquid medium of density ϱ there is an ideal rigid baffle at the plane $z = 0$, with a system N of sound sources. The sources are assumed to be harmonically vibrating circular transducers,

each of thickness h and radius a (Fig. 1). The distance between the centra points of sources 1 and 2 is

$$l_{12} = \sqrt{(x_2 - x_1)^2 + (y_2 - y_1)^2}\,.$$

We can consider a transducer to be a vibrating circular plate of specified thickness, rigidly clamped by its edge to the housing. For this reason we shall take as the basis for assuming a suitable vibration velocity distribution on the surface of the source, an exact mathematical solution of the problem of the free vibration of a circular plate rigidly clamped at its edge.

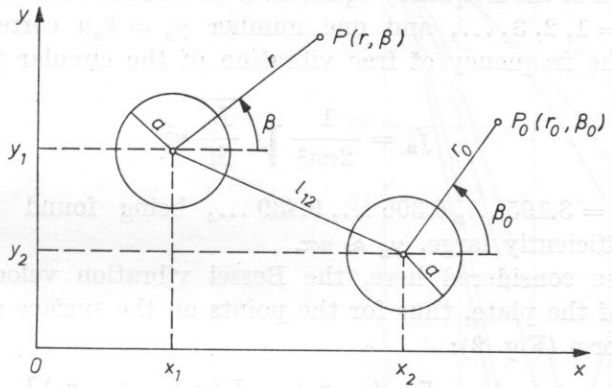

Fig. 1. The coordinate system assumed for the determination of the mutual impedance of circular sources vibrating in a rigid planar baffle

It is known from vibration theory [3] that the transverse axially-symmetric free vibration of a uniform circular plate of a thickness small compared to its radius [2], for vibrations that are harmonic in time, can be described by the equation

$$\zeta(r_0, t) = \zeta_0(r_0)e^{i\omega t} = [A_0 J_0(kr_0) + B_0 I_0(kr_0)]e^{i\omega t}, \tag{1}$$

where $\xi(r_0, t)$ is the displacement of points of the plate in the transverse direction, ω is the angular frequency, t is the time, $i = \sqrt{-1}$, $k^2 = \omega/\sqrt{M/B}$, M is the mass of the plate per unit area, B is the flexural rigidity of the plate and A_0 and B_0 are constants. The special function which occurs here, $I_0(kr_0)$ is a modified Bessel function of the first kind of the zeroth order, which can be described as a Bessel function J_0 of imaginary argument [11], i.e. $I_m(w) = i^{-m} J_m(iw)$.

The boundary conditions for $r_0 = a$ are the following:

1) the plate has zero displacements at the places of rigid clamping:

$$\zeta_0(v_0)|_{r_0=a} = 0; \tag{2}$$

2) and the plate cannot rotate:

$$\frac{d}{dr_0}\zeta_0(r_0)\bigg|_{r_0=a} = 0. \tag{3}$$

For behaviour which is harmonic in time, the vibration velocity distribution $v(r_0, t) = v(r_0)e^{i\omega t}$, with consideration of relations (2) and (3), satisfies the boundary conditions

$$v(r_0)\Big|_{r_0=a} = 0, \qquad \frac{d}{dr_0}v(r_0)\Big|_{r_0=a} = 0,$$

which lead to the so-called frequency equation:

$$J_0(ka)I_1(ka) + J_1(ka)I_0(ka) = 0. \tag{4}$$

The solution of the frequency equation is an infinite series in the quantity k: $k = k_n$ for $n = 1, 2, 3, \ldots$, and one number $\gamma_n = k_n a$ corresponds to each value of k_n. The frequency of free vibration of the circular plate is

$$f_n = \frac{1}{2\pi a^2}\sqrt{\frac{B}{M}}\,\gamma_n^2 \tag{5}$$

with $\gamma_1, \gamma_2, \gamma_3 = 3.195\ldots, 6.306\ldots, 9.439\ldots$, being found for $n = 1, 2, 3$; and, if n is sufficiently large, $\gamma_n \approx n\pi$.

In the case considered here, the Bessel vibration velocity distribution for any point of the plate, thus for the points on the surface of the plate, has the following form (Fig. 2):

$$v_n(r_0) = v_{0n}\left[J_0\left(\gamma_n \frac{r_0}{a}\right) - \frac{J_0(\gamma_n)}{I_0(\gamma_n)} I_0\left(\gamma_n \frac{r_0}{a}\right)\right]. \tag{6}$$

If, however, the vibration source is a circular membrane tensioned with equal force over the whole circumference, then the axially-symmetric free vibration velocity distribution is expressed by the formula (Fig. 2)

$$v_n(r_0) = v_{0n} J_0\left(\beta_n \frac{r_0}{a}\right), \tag{7}$$

where β_n is nth root of the equation

$$J_0(\beta_n) = 0. \tag{8}$$

In this equation $\beta_1, \beta_2, \beta_3 = 2.4048\ldots, 5.5201\ldots, 8.6537\ldots$, and, generally, if n is sufficiently large [11], then $\beta_n \approx n\pi - \pi/4 \approx n\pi$.

The calculation of the mechanical mutual impedance Z_{12} of two planar sound source is carried out on the basis of the definition [5, 9]

$$Z_{12} = \frac{1}{v_{01}v_{02}^*}\int_{\sigma_2} p_{12}(x_0, y_0)v_2^*(x_0, y_0)\,d\sigma_0, \tag{9}$$

where

$$p_{12}(x_0, y_0) = \frac{ik\varrho c}{2\pi}\int_{\sigma_1} v(x, y)\frac{e^{-ikR}}{R}\,d\sigma \tag{10}$$

is the acoustic pressure generated by source 1 and acting on source 2, v_1 is the vibration velocity distribution on the surface of source 1, v_{01} is the amplitude of the vibration velocity of the centre point of source 1, v^* is a quantity coupled in a complex manner with v, $R = \sqrt{(x-x_0)^2+(y-y_0)^2}$ is the distance from the surface element $d\sigma$ on source 1 to the point (x_0, y_0) on source 2.

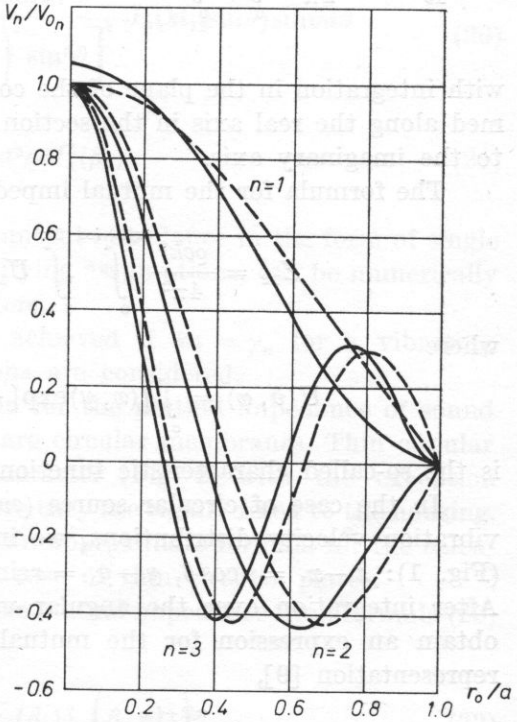

Fig. 2. The plots of the function of the Bessel axial-symmetric vibration velocity distribution for the first three modes: $n = 1$, 2 and 3. The curves of distributions for a circular plate are plotted with a continuous line, the curves for a circular membrane with a discontinuous line

In numerical calculations it is convenient to use the concept of the normalised impedance

$$\frac{Z_{12}}{\lim\limits_{k\to\infty} Z_{11}} = \zeta_{12} = \theta_{12} + i\chi_{12}, \tag{11}$$

where θ_{12}, χ_{12} are, respectively, the normalised mutual resistance and normalised mutual reactance between sources 1 and 2. For $k \to \infty$ we have $p_{11}(x, y) = \varrho c v_1(x, y)$, and then-formula (9) — we obtain

$$\lim_{k\to\infty} Z_{11} = \varrho c \int_{\sigma_1} f_1^2(x, y)\, d\sigma, \tag{12}$$

where $v_1(x, y)/v_{01} = f_1(x, y)$ is a function of the vibration velocity distribution on the surface of source 1.

3. Integral formulae for mutual impedance

In order to facilitate the calculation of the surface integrals (9) and (10), the term e^{-ikR}/R can be represented by a double integral [9],

$$\frac{e^{-ikR}}{R} = \frac{-ik}{2\pi} \int_0^{\pi/2+i\infty} \int_0^{2\pi} \exp\{-ik\sin\vartheta[(x-x_0)\cos\varphi+(y-y_0)\sin\varphi]\}\sin\vartheta d\vartheta d\varphi \tag{13}$$

with integration in the plane of the complex variable $\vartheta = \theta + i\psi$ being performed along the real axis in the section $(0, \pi/2)$ and on the ray $(0, \infty)$ parallel to the imaginary axis.

The formula for the mutual impedance takes the form

$$Z_{12} = \frac{\varrho ck^2}{4\pi^2} \int_0^{\pi/2+i\infty} \int_0^{2\pi} U_1(\vartheta, \varphi)\, U_2^*(\vartheta, \varphi)\sin\vartheta d\vartheta d\varphi, \tag{14}$$

where

$$U(\vartheta, \varphi) = \int_\sigma f(x, y)\exp\{-ik\sin\vartheta(x\cos\varphi + y\sin\varphi)\}d\sigma \tag{15}$$

is the so-called characteristic function of the sound source.

In the case of circular source (each of radius a) with axially-symmetric vibration velocity distributions, we introduce local polar coordinate systems (Fig. 1): $x-x_1 = r\cos\beta$, $y-y_1 = r\sin\beta$, $x_0-x_2 = r_0\cos\beta_0$, $y_0-y_2 = r_0\sin\beta_0$. After integration over the angular variables between the limits $(0, 2\pi)$, we obtain an expression for the mutual mechanical impedance in the Hankel representation [9],

$$Z_{12} = 2\pi\varrho ck^2 \int_0^{\pi/2+i\infty} W(ka\sin\vartheta)\, W^*(ka\sin\vartheta) J_0(kl_{12}\sin\vartheta)\sin\vartheta d\vartheta, \tag{16}$$

where

$$W(ka\sin\vartheta) = \int_0^a f(r_0) J_0(kr_0\sin\vartheta) r_0 dr_0. \tag{17}$$

In the sound source are circular plates, on whose surfaces Bessel type (6) vibration velocity distributions occur, then the normalized mutual impedance [9] is equal to

$$\zeta_{12}^p = \left(2\frac{ka}{\gamma_n}\right)^2 \int_0^{\pi/2+i\infty} \frac{\sin\vartheta J_0(kl_{12}\sin\vartheta)}{\left[1-\left(\frac{ka}{\gamma_n}\right)^4\sin^4\vartheta\right]^2} \times$$

$$\times \left[\frac{J_1(\gamma_n)}{J_0(\gamma_n)} J_0(ka\sin\vartheta) - \frac{ka}{\gamma_n}\sin\vartheta J_1(ka\sin\vartheta)\right]^2 d\vartheta \tag{18}$$

and the normalising factor has the form

$$\lim_{k\to\infty} Z_{11}^{p} = 2\pi a^2 \varrho c J_0^2(\gamma_n). \tag{19}$$

However, when the sound source are circular membranes, we obtain [9]

$$\varrho_{12}^{M} = 2\left(\frac{ka}{\beta_n}\right)^2 \int_0^{\pi/2+i\infty} \frac{J_0^2(ka\sin\vartheta)}{\left[1-\left(\frac{ka}{\beta_n}\right)^2 \sin^2\vartheta\right]^2} J_0(kl_{12}\sin\vartheta)\sin\vartheta d\vartheta \tag{20}$$

with

$$\lim_{k\to\infty} Z_{12}^{M} = \pi a^2 \varrho c J_1^2(\beta_n). \tag{21}$$

The expressions given here for the mutual impedance in the form of single integrals, without using additional simplifying assumptions, can be numerically evaluated only with the use of computers.

Considerable simplification can be achieved if $ka = \gamma_n$ for a vibrating plate, or $ka = \beta_n$ if membrane vibrations are considered.

Formula (20), which is an expression for the mutual impedance of sound sources, is exact only when the sources are circular membranes. Thin circular plates exhibit vibration of the same character (Fig. 2) with the exception of slight deviations close to the edges where they are rigidly fixed to the housing. Thus expression (20) can also be used as an approximate formula for the calculation of the mutual impedance in the case of thin circular plates.

For $ka = \beta_n$, the real component of the mutual impedance from formula (20) takes [9] the form

$$\theta_{12}^{M} = \sum_{p=0}^{\infty} \left(\frac{a}{l_{12}}\right)^p \sigma_p(\beta_n) j_p\left(\beta_n \frac{l_{12}}{a}\right), \tag{22}$$

where

$$\sigma_0(\beta_n) = \frac{1}{2}\beta_n^2 J_1^2(\beta_n),$$

$$\sigma_1(\beta_n) = \left(\frac{\beta_n}{2}\right)^2 J_1(\beta_n) J_2(\beta_n) = \frac{1}{2}\beta_n J_1^2(\beta_n), \tag{23}$$

$$\sigma_p(\beta_n) = \frac{\beta_n}{2} \frac{\Gamma\left(p+\frac{1}{2}\right)}{\sqrt{\pi}} \sum_{q=0}^{p} \frac{J_{q+1}(\beta_n) J_{p-q+1}(\beta_n)}{(q+1)!(p-q+1)!},$$

and [11]

$$j_m(u) \equiv \sqrt{\frac{\pi}{2u}} J_{m+\frac{1}{2}}(u). \tag{24}$$

The imaginary component of the mutual impedance is equal [9] to

$$\chi_{12}^{M} = -\sum_{p=0}^{\infty}\left(\frac{a}{l_{12}}\right)^{p}\sigma_p(\beta_n)n_p\left(\beta_n\frac{l_{12}}{a}\right), \tag{25}$$

where [11]

$$n_m(u) = \sqrt{\frac{\pi}{2u}}N_{m+\frac{1}{2}}(u) \tag{26}$$

is a spherical Neumann function of the mth order. Using the definition for a spherical Hankel function [4] of the second kind

$$h_m^{(2)}(u) = j_m(u) - in_m(u), \tag{27}$$

the normalised mutual impedance of two circular membranes, for $ka = \beta_n$, can be written in the following way:

$$\zeta_{12}^{M} = \sum_{p=0}^{\infty}\left(\frac{a}{l_{12}}\right)^{p}\sigma_p(\beta_n)h_p^{(2)}\left(\beta_n\frac{l_{12}}{a}\right). \tag{28}$$

In order to simplify numerical calculations using formulae (22), (25) or (28), the values of the coefficients $\sigma_p(\beta_n)$ are grouped in Table 1.

Table 1. The expansion coefficients $\sigma_p(\beta_n)$ calculated according to formula (23)

n	σ_0	σ_1	σ_2	σ_3	σ_4	σ_5
1	0.77932	0.32410	0.17557	0.09282	0.03327	0.02073
2	1.76398	0.31955	−0.28180	−0.46808	−0.01840	0.39125
3	2.75907	0.31883	−0.58845	−0.54459	0.34325	1.09679
4	3.75670	0.31859	−0.86487	−0.56872	0.65486	1.35270
5	4.75530	0.31849	−1.13017	−0.57930	0.93842	1.47003

5. Impedance in specific cases

In the cases where $ka \ll \beta_n$ or $ka \ll \gamma_n$, the analysis of the acoustic mutual interaction is considerably simpler since approximate formulae can then be used.

For $(ka/\gamma_n)^4 \ll 1$ we assume the following simplifications in formula (18):

$$\left[1-\left(\frac{ka}{\gamma_n}\right)^4\sin^4\vartheta\right]^{-2} \simeq 1, \quad \left[1-\left(\frac{ka}{\gamma_n}\right)^4\cos h^4\psi\right]^{-2} \simeq 1. \tag{29}$$

The normalised mutual impedance of two vibrating circular plates can

then be reduced [9] to the form

$$\zeta_{12}^{p} = \sum_{p=0}^{\infty} \left(\frac{a}{l_{12}}\right)^{p} \left\{ b_p h_p^{(2)}(kl_{12}) + c_p \left[h_p^{(2)}(kl_{12}) - \frac{2}{kl_{12}} \left(p + \frac{1}{2}\right) h_{p+1}^{(2)}(kl_{12}) \right] + \right.$$

$$\left. + d_p \left[h_p^{(2)}(kl_{12}) - \frac{4}{kl_{12}} \left(p + \frac{1}{2}\right) h_{p+1}^{(2)}(kl_{12}) + \left(\frac{2}{kl_{12}}\right)^2 \left(p + \frac{1}{2}\right)\left(p + \frac{3}{2}\right) h_{p+2}^{(2)}(kl_{12}) \right] \right\}, \quad (30)$$

where

$$b_p = \left(2\frac{ka}{\gamma_n}\right)^2 \frac{\Gamma(p+\frac{1}{2})}{\sqrt{\pi}} \frac{J_1^2(\gamma_n)}{J_0^2(\gamma_n)} \sum_{q=0}^{p} \frac{J_q(ka) J_{p-q}(ka)}{q!(p-q)!}, \quad (30a)$$

$$c_p = -\left(2\frac{ka}{\gamma_n}\right)^3 \frac{\Gamma(p+\frac{1}{2})}{\sqrt{\pi}} \frac{J_1(\gamma_n)}{J_0(\gamma_n)} \sum_{q=0}^{p} \frac{J_{q+1}(ka) J_{p-q}(ka)}{q!(p-q)!}, \quad (30b)$$

$$d_p = 4\left(\frac{ka}{\gamma_n}\right)^4 \frac{\Gamma(p+\frac{1}{2})}{\sqrt{\pi}} \sum_{q=0}^{p} \frac{J_{q+1}(ka) J_{p-q+1}(ka)}{q!(p-q)!}. \quad (30c)$$

If $ka/\gamma_n \ll 1$, then in formula (30) we need consider only the term containing the coefficient b_p, neglecting the terms which contain the coefficients c_p and d_p. Then

$$\zeta_{12}^{p} = \sum_{p=0}^{\infty} \left(\frac{a}{l_{12}}\right)^{p} b_p h_p^{(2)}(kl_{12}). \quad (31)$$

The calculations of the mutual impedance are less complicated if the sound sources are vibrating circular membranes. In this case for $(ka/\beta_n)^2 \ll 1$ we obtain

$$\zeta_{12}^{M} = \sum_{p=0}^{\infty} \left(\frac{a}{l_{12}}\right)^{p} b_p h_p^{(2)}(kl_{12}), \quad (32)$$

where

$$b_p = a_n b_p', \qquad a_n \equiv 2\left[\frac{\beta_n}{\gamma_n} \frac{J_1(\gamma_n)}{J_0(\gamma_n)}\right]^2. \quad (33)$$

For the first successive Bessel modes ($n = 1$ 2 and 3) the coefficients a_n are equal to: $a_1 = 0.7724\ldots$, $a_2 = 1.2969\ldots$, $a_3 = 1.4997\ldots$, while $\lim_{n\to\infty} a_n = 2$.

From relations (31)-(33) we obtain

$$\zeta_{12}^{p} = a_n \zeta_{12}^{M} \quad (34)$$

for $ka \ll \gamma_n$ and $(ka)^2 \ll \beta_n^2$. This means that for the first Bessel mode the mutual impedance of the plates is smaller than the mutual impedance of the membranes. However, for the second and higher modes the mutual impedance of the plates is smaller than that of the membranes.

If we assume that $ka \ll 1$, then in formulae (31) and (32) we consider

only the element of the zeroth order ($p = 0$), neglecting the remaining elements as small quantities of higher orders. We then obtain

$$\zeta_{12}^{p} \simeq \theta_{11}^{p}\left[\frac{\sin(kl_{12})}{kl_{12}} + i\,\frac{\cos(kl_{12})}{kl_{12}}\right], \tag{35}$$

$$\zeta_{12}^{M} \simeq \theta_{11}^{M}\left[\frac{\sin(kl_{12})}{kl_{12}} + i\,\frac{\cos(kl_{12})}{kl_{12}}\right], \tag{36}$$

where the quantities

$$\theta_{11}^{p} \simeq \left(2\frac{ka}{\gamma_n}\right)^2 \frac{J_1^2(\gamma_n)}{J_0^2(\gamma_n)}, \qquad \theta_{11}^{M} \simeq 2\left(\frac{ka}{\beta_n}\right)^2 \tag{37}$$

are the expressions for normalised self-resistances, provided $ka \ll 1$.

6. The analysis of the results

In the numerical examples, the mutual impedance of the two kinds of source was considered:

a) circular membranes,

b) circular plates rigidly clamped at the circumference.

The impedance was calculated for Bessel axially-symmetric vibration velocity distributions shown, using formulae (7) in the case of the membranes, and formula (6) for plates.

If $ka \gg 1$, the approximate formulae (35)-(36) can be used. In practice, this approximation is valid if $ka < 0.2$.

The calculation of the mutual impedance on the basis of formula (30) or (32) involves a relative error of less than 5 % if $ka < 1/3\gamma_n$, $1/3\beta_n$.

In the case of the frequencies of resonance, i.e. for $ka = \beta_n$, formula (28) is convenient for the calculation of the mutual impedance of the membranes.

If $ka \gg \gamma_n, \beta_n$, the real component of the normalized mutual impedance is close to unity; the imaginary component, however, is close to zero.

In the other cases, when the approximations cannot be used, or when great exactness of results is required, the calculation can be performed using computers on the basis of the integral formulae (18) and (20).

The practical formulae for numerical calculations of the self-impedance of one membrane or one plate, can be obtained from the integral formulae (18) and (20). This problem was analyzed in reference [9].

On the basis of the results obtained from the investigation of the problem of the mutual impedance of the Bessel axially-symmetric modes of vibrating circular plates, clamped at the circumference, or vibrating circular membranes, the following conclusions can be formulated:

1. The mutual impedance of two sound sources depends predominantly on the distance l_{12} between the central points of the sources.

The real and imaginary components of the mutual impedance oscillate around a value of zero, i.e. take extreme values that are alternately positive and negative, where the oscillations decay as the distance between the sources increases (Fig. 3). The curves of the mutual resistance are shifted relative to the reactance curves (Figs. 3-5). When the linear dimensions of the sources are smaller than the acoustic wavelength, then the mutual impedance depends on the distance l_{12} through the function $e^{-ikl_{12}}/kl_{12}$, where $k = 2\pi/\lambda$. This regularity is valid in the case of the mutual reactance with an additional assumption that $l_{12} > 0$.

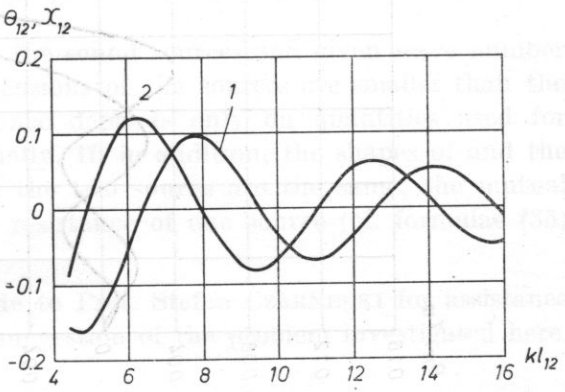

Fig. 3. The normalised mutual impedance of two vibrating circular membranes for the first axial-symmetric Bessel mode ($m = 0$, $n = 1$), depending on the parameter kl_{12} for $ka = 2.2$

Curve *1* – resistance, curve *2* – reactance

2. The mutual impedance for a given distance between sources and given sizes of sources, is an oscillating function of frequency, oscillating about a value of zero.

The extreme values of the mutual impedance of vibrating circular plates or vibrating circular membranes, occur for values of ka close, respectively, to γ_n or β_n (Figs. 4 and 5).

In the case of higher Bessel functions, i.e. when n is sufficiently large, the approximation $\beta_n \simeq \gamma_n \simeq n\pi$ gives us the simple relation $n\lambda \simeq 2a$ in place of $(2\pi/\lambda) \simeq a\beta_n$ and $(2\pi/\lambda)a \simeq \gamma_n$. It also seems characteristic that the acoustic interaction decays rapidly for wavelengths only slightly different from the value $2a/n$. For example, for the fifth axially-symmetric Bessel mode ($n = 5$, $\lambda \simeq 2a/5$), the largest acoustic interaction occurs for a narrow range of wavelengths which are only slightly different from the value $\lambda = 2a/5$. Outside this narrow radiation band, the acoustic interaction decays violently.

3. The form of the vibration velocity distribution on the surface of the sources affects the size and behaviour of the variation in the mutual impedance.

For given source size and separation the acoustic interaction becomes greater, as the active surfaces of the sources become greater.

The highest values of the mutual impedance occur for the first mode (Fig. 4), for successively higher Bessel modes (cf. Figs. 4 and 5) the extreme values become lower and are shifted towards shorter wavelength. This property

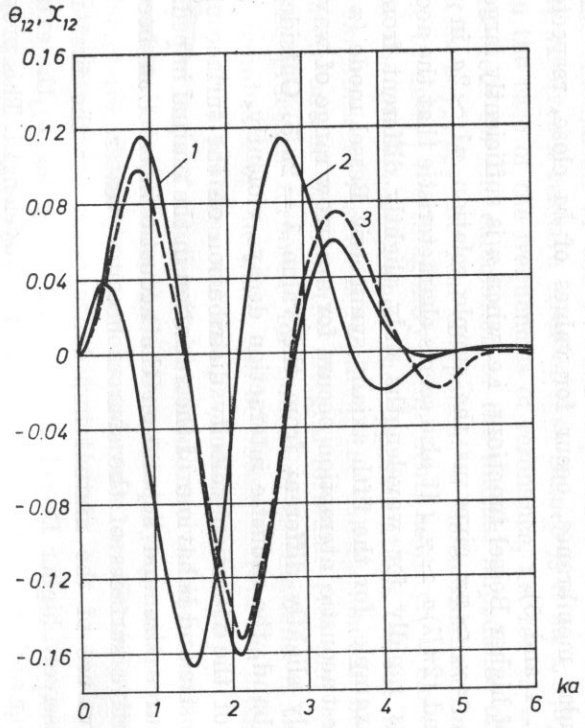

Fig. 4. The normalised mutual impedance of two circular sound sources for the first axial-symmetric Bessel mode ($m = 0$, $n = 1$)

Curve *1* – the resistance of the membrane, curve *2* – the reactance of the membrane, curve *3* – the resistance of the plate clamped at the circumference. It was assumed that $a/l_{12} = 0.44$

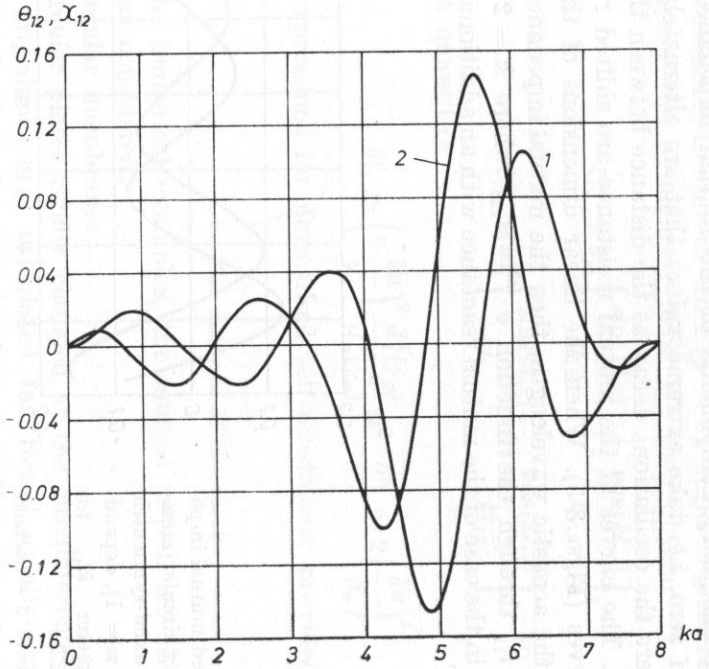

Fig. 5. The normalised mutual impedance of circular membranes for the second axial-symmetric Bessel mode ($m = 0$, $n = 2$)

Curve *1* – resistance, curve *2* – reactance. It was assumed that $a/l_{12} = 0.44$

can be clearly seen for the second and higher Bessel modes, for which the elements of the surface of the source (circular rings) vibrate with opposite phases. This is conditioned by the size of the active area of the sources, which becomes smaller with higher order Bessel modes.

4. Increasing the sizes of sources can be used to obtain an increase in the extreme values of the mutual resistance and reactance.

The limited range of variation in this quantity should be considered in the investigation of the dependence of the mutual impedance on the linear dimensions of the sources. For example, for circular sources (each of the radius a), with the centre points of the sources separated by l_{12}, the condition $0 \leqslant 2a \leqslant l_{12}$ occurs.

For a given distance between the sound sources and given wave number $k = 2\pi/\lambda$, provided the linear dimensions of the sources are smaller than the wavelength λ, the mutual impedance depends only on quantities used for characterizing each source individually. If, in addition, the shapes of and the vibration velocity distributions on the two source are the same, the mutual impedance depends on the self – resistance of one source (cf. formulae (35) and (36)).

I wish to express my gratitude to Prof. Stefan CZARNECKI for assistance in the scientific research and the suggestion of the problem investigated here.

References

[1] K. C. CHAN, *Mutual acoustic impedance between flexible disks of different sizes in an infinite rigid plane*, JASA, **42**, 5, 1060-1063 (1967).

[2] I. MALECKI, *Theory of waves and acoustic systems* (in Polish), PWN, Warszawa 1964.

[3] N. W. MCLACHLAN, *Bessel functions for engineers*, PWN, Warszawa 1964.

[4] P. M. MORSE, H. FESHBACH, *Methods of theoretical physics*, vol. 1 and 2, McGraw-Hill, New York 1953.

[5] D. T. PORTER, *Self – and mutual – radiation impedance and beam patterns for flexural disks in a rigid plane*, JASA, **36**, 6, 1154-1161 (1964).

[6] W. RDZANEK, *Mutual impedance of an array of circular pistons with gaussian distribution of vibration velocity*, Acta Physica Polonica, **A-42**, 5, 623-625 (1972).

[7] W. RDZANEK, *Mutual impedance of a system of flat circular transducers with a given vibration velocity amplitude distribution* (in Polish), Wydawnictwo Uczelniane 1-78 (1973).

[8] W. RDZANEK, *Mutual impedance of an array if circular pistons with a given distribution of vibration velocity*, Acta Physica Polonica, **A-45**, 2, 299-302 (1974).

[9] W. RDZANEK, *Mutual and total acoustic impedance of a system of sources with a variable surface distribution of particle velocity* (in Polish), Wydawnictwo Uczelniane WSP (1979).

[10] W. RDZANEK, *The mutual acoustic impedance of circular panels with the Bessel distribution of vibration velocity*, Proc. XXV Open Seminar on Acoustics Poznań-Błażejewko 1978.

[11] G. N. WATSON, *Theory of Bessel functions*, 2nd ed., University Press Cambridge 1966.

Received on March 27, 1979; revised version on November 22, 1980.

ARCHIVES OF ACOUSTICS
5, 3, 251-260 (1980)

GENERATION AND DETECTION OF INCOHERENT HYPERSONIC VIBRATIONS USING SUPERCONDUCTING TUNNEL JUNCTIONS

MIKOŁAJ ALEKSIEJUK, MIECZYSŁAW M. DOBRZAŃSKI

Institute of Fundamental Technological Research of the Polish Academy of Sciences
(00-049 Warszawa, ul. Świętokrzyska 21)

WIESŁAW LARECKI

Institute of Radioelectronics of Warsaw Technical University
(00-665 Warszawa, ul. Nowowiejska 15/13)

The investigations of superconducting tunnel junctions as phonon generators and detectors are reported. Theoretical predictions and the published results of the experimental research on such devices are briefly reviewed. The experimental results of the investigations of the current-voltage characteristics of fabricated tin tunnel junctions are presented and discussed, and then the measured current-signal transmission characteristics of pairs of identical tunnel junctions deposited on the corundum sample are analyzed and interpreted. The results obtained are compared with the results o similar investigations reported in the literature.

1. Introduction

The process of the generation and detection of phonons in superconducting devices is based on the production of nonequilibrium (quasi-equilibrium) states in thin superconducting layers. In general, the nonequilibrium states of the superconducting layer can be produced by the injection of electrons, phonons or photons.

In the case of a detector, the nonequilibrium state is produced by a flux of incident phonons, while in the case of a generator the external source of energy produces an excess population of quasiparticles. Of the various methods for producing nonequilibrium population of quasiparticles in superconducting layers, superconducting tunnel junctions [1, 2], the a.c. Josephson effect [3],

and the "phonon fluorescence" effect [4, 5], (i.e. the effect of thermal pulses) have been used to generate phonons, while the possibility of using laser light was noted in [6].

Since a conversion of the energy of the external source into the energy of the phonons occurs in a superconducting generator, it is possible to obtain the similar intensity of the flux of phonons generated for each of the methods, because it is limited by the possibility of destruction of the superconducting state. The superconducting devices used for phonon detection are superconducting tunnel junctions [2] and bolometers [1]. The general model and the related quantitative description of the performance of detectors and generators with superconducting elements must therefore be based on the equations of dynamic equilibrium of the kinetic processes occurring in a nonequilibrium superconductor. It is assumed that the time scale of the action of the external source, which produces the nonequilibrium is several orders of magnitude greater than the time scale of the kinetic processes in the superconductor itself — and thus it can be assumed that we are concerned here only with the steady states of the nonequilibrium superconductor. The general equations of dynamic equilibrium balance of the superconductor were derived in [7] and developed in [8]. These equations are valid for macroscopic densities of phonons and quasiparticles and they do not determine the energy distributions of these excitations.

In order, however, to determine the spectrum and possibly also the intensity of the flux of phonons generated, or the variation of the detector current caused by a given incident flux of phonons, it is necessary to know the distributions of the quasiparticles and phonons and the characteristic times of the kinetic processes in the layer of the nonequilibrium superconductor under investigation. These quantities can be calculated from solutions of the coupled balance and kinetic equations and from the gap equation of a nonequilibrium superconductor. Such equations were derived in [9], with the assumption that the processes of scattering and recombination of quasiparticles and phonon trapping are equally significant in the nonequilibrium superconductor [10].

In previous models of a nonequilibrium superconductor [11, 12] it was assumed that scattering is the main mechanism of the relaxation processes. In [9], however, only a linearized form of these equations was derived, with the assumption of relatively low energy of the injected excitations i.e. weak nonequilibrium and, thus ignoring electron—electron interactions, which are essential for quasiparticles of large energies, and also assuming that the superconducting layer is "thin" i.e. phonon escope time is independent of phonon energy. Thus the applicability of [9] for actual generators and detectors of phonons depends on the satisfaction of these assumptions.

The problem of a nonequilibrium superconductor has not yet been solved for the general case, and it is not therefore possible to present a general model for a superconducting generator and detector of phonons.

Application of superconducting tunnel junctions for the generation and detection of incoherent phonons was developed in early 1970's [5, 12, 14-20]. In this paper we present the results of the experimental investigations related to the technique of manufacturing superconducting tunnel junctions and the results of the observations of the current-signal characteristics of two identical junctions on a sample of Al_2O_3 (corundum) operated with low modulation of the generator current [5]. These results are compared with the published experimental investigations and with the theoretical predictions.

2. The superconducting tunnel junction as a generator and detector of phonons

The papers concerning the application of superconducting tunnel junctions for the generation and detection of phonons, in addition to the results of experimental investigations, have also presented same attempts to build a theoretical model of such devices in order to calculate the spectrum of the emitted phonons and the transmission characteristics. The calculations of the spectrum of the emitted phonons [13, 14], and of the transmission characteristics of tunnel generator–tunnel detector system [16] were performed on the basis of a model of a equilibrium superconductor at zero temperature [21]. This required the assumption of a negligibly low density of injected excitations compared to the equilibrium density, and also that the phonons produced in the relaxation and recombination of the excess quasiparticles are not trapped.

In [19] and subsequently in [5], a quantitative description of the generator detector system was based on the balance equations [7] and on a simplified model of the generator and detector, assuming three possible energy levels for the quasiparticles and the same functions for the density of the quasiparticles and phonons as for an equilibrium superconductor, which in consequence gave an "artificial" root singularity in the "theoretical curves".

In the case of moderate quasiparticle injection generator current and relatively low temperatures good agreement of the calculated and experimental results was achieved for Al–I–Al [15] and Pb–I–Pb [19] junctions, while in the case of Sn–I–Sn junctions the discreponcy was significant [5].

A description of a nonequilibrium superconductor was attempted in [18], using discrete levels for the states of the quasiparticles and phonons, and on the basis of detailed balances of the velocities of escape and scattering of phonons and of pair breaking by phonons the energy spectrum, i.e. the width of the recombination peak of the phonons emitted by a tunnel generator operated in the low intensity range $V < 4\Delta/e$ (where 2Δ is the width of energy gap, and e is the charge of the electron) was found by numerical calculation.

The calculated results were compared with the experimental results for a Sn–I–Sn junction and gave good agreement.

The phenomenon of resonance absorption of phonons by the donor levels of Sb in a uniaxially stressed smaple of Ge: Sb was used in [5, 16] for an experi-

mental determination of the spectrum of the phonons emitted by the superconducting tunnel junctions.

The problem of an appropriate and full theoretical model for superconducting generator and detector of phonons has not yet been solved to the authors knowledge and thus the first stage of the investigations undertaken was limited to an experimental investigation. It seems, however, that the approach proposed in [9, 22] may prove fruitful in theoretical analyses.

3. The experimental investigation of a system of tunnel junctions

The superconducting tunnel junctions used for the generation and detection of phonons are usually made of tin (Sn) [2, 5, 13, 18], lead (Pb) [16] or aluminium (Al) [15]. The use of aluminium, requires a working temperature below 1K, because of its relatively low critical temperature and this causes some technical difficulties. Junctions made of tin and lead can work effectively at slightly higher temperatures, with the former giving a better signal to noise ratio in the measurements, because of the lower recombination velocity, compared to that of lead. Tin tunnel junctions were therefore used in the present investigations. The junctions had the form of two thin layers, 2000 A thick, between which there was a dielectric barrier of tin oxides (Sn_xO_y) approximately 20 Å thick. The surface area of the junction was 1 mm². The sample was a single corundum crystal (Al_2O_3) of dimensions $7 \times 7 \times 4$ mm³. Thin layers of Sn were deposited successively in a vaccuum apparatus, and the oxide barrier was obtained by oxidining the first (bottom) layer of Sn in the atmosphere, with the barrier thickness being controlled by varying the time of oxidation. In the normal state, the resistances of the junctions prepared did not exceed 0.3 Ω. The junctions were placed on the largest opposite sides of the sample perpendicular to the c-axis of the single crystal. The sample with the junctions is shown in Fig. 1. The sample with the junctions was clamped, providing electrical connections, and the whole was placed in a metal container immersed in liquid helium. A typical cryostat equipped with a booster pump was used, in which temperatures from 4.2 K to 1.8 K were obtained by helium evaporation.

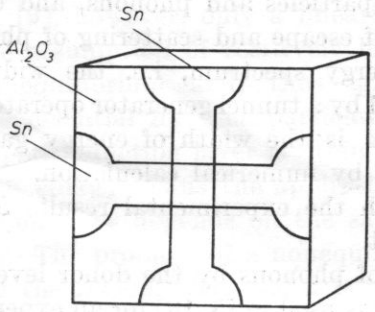

Fig. 1. $AnAl_2O_3$ single crystal sample with $Sn-(Sn_xO_y)-Sn$ junctions

Investigation of the tunnel junctions

The investigations of the current-voltage characteristics of the manufactured junctions were performed by the four point method using an X-Y recorder. The aim of these measurements was to examine the correctness of the junction fabrication and to find the point on the characteristic at which the junction would be operated as phonon detector, i.e. the voltage $V < 2\Delta/e$ in the vicinity of which the $I(V)$ characteristic is approximately most linear.

An example of the $I(V)$ characteristic of a junction operated at a temperature of 1.8 K used for both phonon detection and generation is shown in Fig. 2.

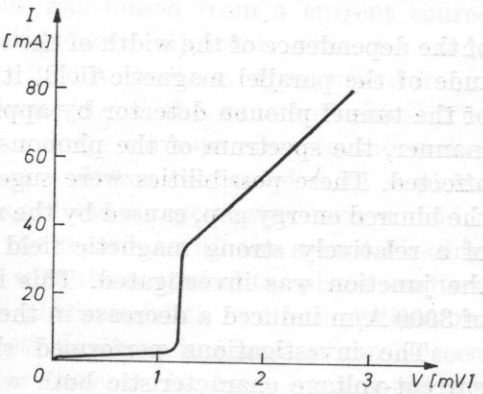

Fig. 2. The current-voltage characteristic of the Sn – (Sn_xO_y) – Sn junction at a temperature $T = 1.8$ K

From the current-voltage characteristic of a junction the width of the energy gap can be evaluated and for the characteristic shown in Fig. 2, $2\Delta = 1.2$ meV. Since all the Josephson effects occurring in a superconducting tunnel junction can be suppressed by the application of a low magnetic field parallel to the superconducting layers, thus reducing the "zero current" of the detecting junction, the influence of a low magnetic field on the current-voltage characteristic of fabricated junctions was determined. The results of these investigations are shown in Fig. 3. It can be seen in the figure that for $H = 40$ A/m the "zero current" decreases more than three times. As a result

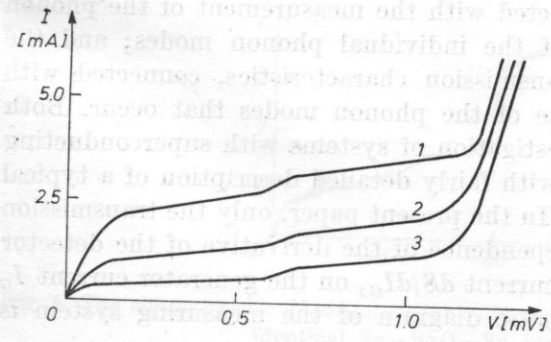

Fig. 3. The current-voltage characteristics of the Sn – SnO – Sn junction for weak magnetic fields

$1 - H = 0$, $2 - H = 20$ A/m, $3 - H = 40$ A/m. The magnetic field H was paralell to the plane of the junction; $T = 1.8$ K

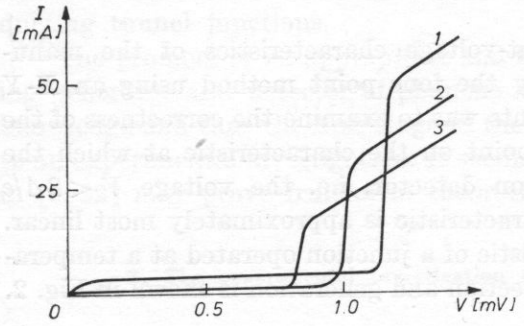

Fig. 4. The current-voltage characteristics of the junction for strong magnetic fields $1 - H = 0$, $2 - H = 2000$ A/m, $3 - H = 3000$ A/m; $T = 1.8$ K

of the dependence of the width of the superconduction energy gap on the magnitude of the parallel magnetic field, it is possible to tune the energy threshold of the tunnel phonon detector by applying the magnetic field. In an analogous manner, the spectrum of the phonons emitted by the tunnel generator can be affected. These possibilities were sugested in [14], although it was noted that the blurred energy gap, caused by the magnetic field occurs. Thus, the influence of a relatively strong magnetic field on the current-voltage characteristic of the junction was investigated. This is illustrated in Fig. 4. A magnetic field of 3000 A/m induced a decrease in the energy gap of approximately 30 percent.

The investigations performed show that the junctions had "correct" current-voltage characteristic both without an external magnetic field and in the presence of a magnetic field. The "zero current" of these junctions (i.e. the current for $V < 2\Delta/e$) was, however, much higher than the "zero current" of the similar junctions used, for example, in [5, 23]. This may have been caused by a slightly higher working temperature, and also by the possible existance of "point" breakdowns of the isolating barrier.

Investigation of the transmission characteristics

In the investigation of a superconducting phonon generator – material sample – superconducting phonon detector system, two basic methods have been used: the pulse method, connected with the measurement of the phonon arrival times and the separation of the individual phonon modes; and the method of the measurement of transmission characteristics, connected with the integration with respect to time of the phonon modes that occur. Both methods have been used in the investigation of systems with superconducting tunnel junctions [2, 13, 14, 18, 20], with fairly detailed description of a typical measurement set being given in [5]. In the present paper, only the transmission characteristics in the form of the dependence of the derivative of the detector signal with respect to the generator current dS/dI_G, on the generator current I_G have been investigated. The schematic diagram of the measuring system is

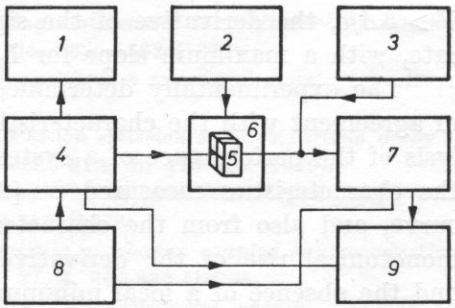

Fig. 5. A block diagram of the measuring system

1 – digital voltage indicator, *2* – electromagnet supply, *3* – bias source, *4* – saw-tooth voltage generator, *5* – the sample with junctions, *6* – electromagnet, *7* – phase sensitive detector, *8* – low-frequency generator, *9* – *X-Y* recorder

shown in Fig. 5. The generating junction was biased from a current source with a saw-tooth waveform, whose rise time was adjustable over the range 5 to 50 s, and amplitude over the range 0 to 2 A. A small a.c. signal with a frequency of approximately 130 Hz was superposed on the saw-tooth bias. The detecting junction was biassed by a d.c. voltage corresponding to the earlier determined working point of the junction and was connected with a phase sensitive detector adjusted to the frequency of the a.c. generator current modulation. The connection of the input X of the recorder with the source biassing the generating junction and of the input Y with the output of the phase sensitive detector permits direct recording of the characteristics under investigation. An example of the transmission characteristic is shown in Fig. 6. It can be seen from Fig. 6 that over the range of generator currents, I_G, from 1 mA to 60 mA corresponding to voltages $2\Delta/e < V < 4\Delta/e$ the derivative of the signal rises slightly, nearly linearly with increasing current. The jump in the derivative, whose slope depends on the magnitude of the modulation of the generator current and corresponding to a generator voltage $V = 4\Delta/e$, occurs at a current $I_G = 60$ mA. For currents I_G between 60 mA and 90 mA corresponding to voltages $4\Delta/e < V < 6\Delta/e$ the derivative of the signal is nearly constant. As the current increases above 90 mA, which corresponds to the voltage range

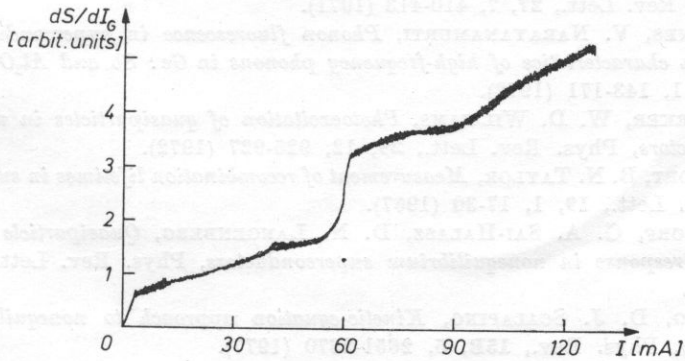

Fig. 6. The characteristic dS/dI_G as a function of the generator current for a system of two identical Sn – SnO – Sn junctions at $T = 1.8$K

$V > 6\Delta/e$, the derivative of the signal increases monotonically at a varying rate, with a maximum slope for I_G −90 mA, i.e. $V = 6\Delta/e$.

The experimentally determined transmission characteristics are basically in agreement with the characteristics expected from a rather qualitative analysis of the performance of a system of junctions, and also in agreement with the characteristics measured in [2, 5]. Some differences from the expected curve, and also from the characteristic measured in [18], involving a slight monotonical rise of the derivative for generator voltages $2\Delta/e < V < 4\Delta/e$, and the absence of a local minimum of the derivative over the voltage range $4\Delta/e < V < 6\Delta/e$ most probably results from the resistance of the junctions in the normal state being much higher than in [18], and from a much higher "zero current" of the junctions used, which in turn is connected with the much higher working temperature of the system compared to that in [18] and to undamped Josephson effects. The sensitivity of the measuring apparatus used, the magnitude of the signal modulating the current of the junction and the electrical matching of the individual elements of the measuring system may also be of some significance.

The authors wish to thank the Director of the Physics Institute of Polish Academy of Sciences for providing the possibilities of performing the experiments and Grzegorz JUNG for fabricating the tunnel junctions.

References

[1] W. EISENMENGER, *Emission, absorption and propagation of acoustic THz waves in solids*, Archives of Acoustics **4**, 2, 141-156 (1979).

[2] W. EISENMANGER, A. M. DAYEM, *Quantum generation and detection of incoherent phonons in superconductors*, Phys. Rev. Lett., **13**, 4, 125-127 (1967).

[3] H. KINDER, *Phonon generation by the a.c. Josephson effect*, Phys. Lett., **36A**, 5, 379-380 (1971).

[4] V. NARAYANAMURTI, R. C. DYNES, *Intense tunable phonon fluorescence in superconductors*, Phys. Rev. Lett., **27**, 7, 410-413 (1971).

[5] R. C. DYNES, V. NARAYANAMURTI, *Phonon fluorescence in superconductors and the propagation characteristics of high-frequency phonons in Ge: Sb and* $Al_2O_3: V^{3+}$, Phys. Rev., **6B**, 1, 143-171 (1972).

[6] W. H. PARKER, W. D. WILLIAMS, *Photoexcitation of quasiparticles in nonequilibrium superconductors*, Phys. Rev. Lett., **29**, 12, 925-927 (1972).

[7] A. ROTHWORT, B. N. TAYLOR, *Measurement of recombination lifetimes in superconductors*, Phys. Rev. Lett., **19**, 1, 17-30 (1967).

[8] A. ROTHWORF, G. A. SAI-HALASZ, D. N. LANGENBERG, *Quasiparticle lifetimes and microwave response in nonequilibrium superconductors*, Phys. Rev. Lett., **33**, 4, 212-215 (1974).

[9] J-J. CHANG, D. J. SCALAPINO, *Kinetic-equation approach to nonequilibrium superconductivity*, Phys. Rev., **15B**, 5, 2651-2670 (1977).

[10] S. B. KAPLAN, C. C. CHI, D. N. LANGENBERG, J-J. CHANG, S. JAFAREY, D. J. SCALAPINO, *Quasiparticle and phonon lifetimes in superconductors*, Phys. Rev., **14B**, 11, 1, 4854-4873 (1976).

[11] C. S. Owen, D. J. Scalapino, *Superconducting state under the influence of external dynamic pair breaking*, Phys. Rev. Lett., **28**, 24, 1559-1562 (1972).

[12] W. H. Parker, *Modified heating theory of nonequilibrium superconductors*, Phys. Rev., **12B**, 9, 3667-3672 (1975).

[13] H. Kinder, K. Laszman, W. Eisenmenger, *Phonon emission by quasiparticle decay in superconducting tunnel junctions*, Phys. Lett., **31A**, 8, 475-476 (1970).

[14] H. Kinder, *Spin-phonon coupling of Al_1O_3 and V^{3+} by quantitative spectroscopy with phonons*, Zeitschrift für Physik, **262**, 4, 295-314 (1973).

[15] A. R. Long, C. J. Adkins, *Transfer characteristics of phonon coupled superconducting tunnel junctions*, The Philosophical Magazine, **27**, 4, 865-882 (1973).

[16] R. C. Dynes, V. Narayanamurti, M. Chin, *Monochromatic phonon propagation in Ge: Sb using superconducting tunnel junctions*, Phys. Rev. Lett., **26**, 4, 181-184 (1971).

[17] H. J. Trumpp, K. Laszman, W. Eisenmenger, *Transition of 280 GHz phonon from superconducting tunnelling junctions into liquid helium and silicon*, Phys. Lett., **41A**, 5, 431-432 (1972).

[18] A. H. Dayem, J. J. Wiegand, *Emitted phonon spectrum and its influence on the detected signal in superconducting Sn diodes*, Phys. Rev., **5B**, 11, 4390-4403 (1972).

[19] A. H. Dayem, B. I. Miller, J. J. Wiegand, *Phonon generation and detection in superconducting lead diodes*, Phys. Rev., **3B**., 9, 2949-2961 (1971).

[20] H. Kinder, *Spectroscopy with phonons on $Al_2O_3: V^{3+}$ using the phonon bremsstrahlung of superconducting tunnel junction*, Phys. Rev. Lett., **28**, 24, 1564-1567 (1972).

[21] L. Tewordt, *Life times of quasi-particles and phonons in superconductors at zero temperature*, Phys. Rev., **127**, 2, 371-382 (1962).

[22] J-J. Chang, D. J. Scalapino, *Tunnelling as a probe of nonequilibrium superconducting states*, Phys. Rev., Lett., **37**, 9, 522-526 (1976).

[23] P. Hu, R. C. Dynes, V. Narayanamurti, *Dynamics of quasiparticles in superconductors*, Phys. Rev., **10B**, 7, 2786-2788 (1974).

Received on March 20, 1980.

ARCHIVES OF ACOUSTICS
5, 3, 261-274 (1980)

GENERATION OF ACOUSTO-ELECTRICAL WAVES USING A SOURCE OF TRANSVERSE VIBRATIONS

NGUYEN VIET KINH, W. PAJEWSKI

IPPT PAN (00-049 Warszawa, ul. Świętokrzyska 21)

The paper presents a theoretical analysis of the generation of transverse surface waves, using a linear source of vibrations, placed in the plane in which the generated wave propagates. On the basis of the results of the theory presented, the problem of the generation of a surface wave excited by a source of finite dimensions in the form of piezoelectric plates is considered. This method of wave generation was used for the generation of transverse surface waves on a piezoelectric ceramic and on niobiate and iodate of lithium.

1. Introduction

Transverse surface waves are generated when the velocity of bulk transverse waves close to the surface decreases. This phenomenon may be caused by a decrease in the stiffness of a material, or an increase in the density in the surface layer. Such boundary conditions exist, for example, in the case of a piezoelectric material whose stiffness depends on the electric field. Waves of this type were described by BLEUSTEIN [1] and independently by GULAEV [3], in 1968. At present, with the progress in the technology of materials whose surface layer has different properties from the properties of the other parts of the material, surface waves can useful for the investigation of the properties of these layers [11]. In the case of piezoelectric materials, the investigation of surface transverse *B. G.*, also called acousto-electrical, waves is very advanced [2, 4-6]. The source of these waves is usually an interdigital transducer to which a variable electric field is applied and which, through the piezoelectric effect, generates an elastic wave. The theoretical methods of solving the problem of the generation of acousto-electric waves are based on the calculus of variations [9] and the use of the Fourier integral [9].

In addition to the above methods for the generation of surface waves

using an electric field, it is possible to excite waves by the application of a suitable source of mechanical vibration on either a piezoelectric material or a nonpiezoelectric material with a layer structure. This method of exciting transverse surface acoustic waves permits a broadening of the range of their use in the investigation of the surface layers of materials treated using modern technologies.

The subsequent parts of the paper will discuss the theoretical side of the problem, and some experimental investigations performed using known piezoelectric materials.

2. Generation of transverse surface waves using a source of transverse vibrations

The paper analyzes the following cases:

a. a linear source of transverse vibrations on the surface of wave propagation,

b. a plate source of transverse vibrations on the surface of wave propagation,

c. a plate source on a surface perpendicular to the surface of wave propagation.

The methods for the analysis of these three cases are similar. Therefore, the first case considered will be the simplest: that of a linear source, where the wave propagates on a piezoelectric material with a free surface or a surface covered by a thin metal layer with very small mass and stiffness.

Using the coordinate system shown in Fig. 1, and assuming that the surface of piezoelectric material is covered with metal layer, we take the direction X_1 as the direction of surface wave propagation; the vibration direction coincides with the X_3 axis, which is an axis of twofold symmetry for a $LiIO_3$ crystal, and the polarisation axis for a ceramic. We look for a component of the vector displacement in the X_3 direction on the surface $X_2 = 0$, caused by the linear source. For the case of a ceramic, the boundary conditions are the following:

$$T_{23}|_{X_2=0} = C_{44}^{E} \frac{\partial U_{3m}^{(1)}}{\partial \chi_2} = \delta(X_1) e^{-j\omega t}, \tag{1}$$

$$\Phi|_{X_2=0} = \frac{e_{15}}{\varepsilon_{11}^{5}} U_{3m}^{(1)} + \varphi|_{X_2=0} = 0, \tag{2}$$

where $U_{3m}^{(1)}$ is the component of particle displacement in the X_3 direction for the metal surface and $\delta(x)$ is the Dirac function.

$U_{3m}^{(1)}$ and Φ satisfy the following conditions

$$C_{44}^{E} \nabla^2 U_{3m}^{(1)} + e_{15} \nabla^2 \Phi = \varrho \ddot{U}_3, \tag{3}$$

$$e_{15} \nabla^2 U_{3m}^{(1)} - \varepsilon_{11}^{S} \nabla^2 \Phi = 0. \tag{4}$$

C_{44}^E, e_{15}, ε_{11}^S are, respectively, the elastic, piezoelectric and dielectric constants, Φ is the electric potential connected with the electric field, $E = -\text{grad}\,\Phi$ and φ is a potential satisfying the following equation:

$$\frac{\partial^2\varphi}{\partial^2 X_1^2} + \frac{\partial^2\varphi}{\partial^2 X_2^2} = 0. \tag{5}$$

It is well known that the vector of displacement of a particle of the medium can be written, in general, as

$$\vec{V} = \text{grad}\,\tau + \text{rot}\,\psi. \tag{6}$$

τ and ψ are the scalar and vector potentials of the acoustic field. Since the required wave is a plane transverse wave, $\tau \equiv 0$ and ψ has only one component $\psi_y \equiv \psi(X_1, X_2)$. Expression (6) takes the form

$$U_{3m}^{(1)} = \frac{\partial\psi}{\partial X_1}. \tag{7}$$

$\psi(X_1, X_2)$ satisfies the equation

$$\frac{\partial^2\psi}{\partial X_1^2} + \frac{\partial^2\psi}{\partial X_2^2} + k_t^2\psi = 0, \tag{8}$$

where $k_t = \omega/C_t$ is the wave number of the transverse wave in the material which is stiffened as a result of the piezoelectric effect

$$C_t = \sqrt{\frac{C_{44}^E}{\varrho}(1+K^2)}$$

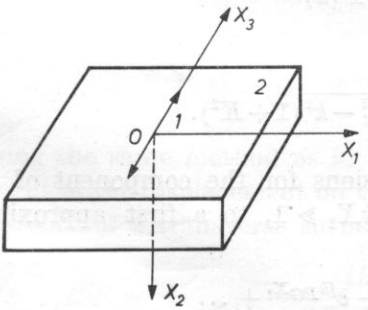

Fig. 1. A linear source with transverse vibration on the surface of wave propagation

1 – linear source, *2* – the surface of wave propagation

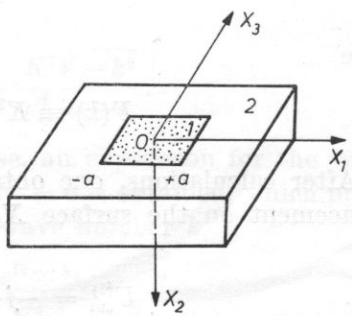

Fig. 2. A plate source with transverse vibration on the surface of wave propagation

1 – plate source, *2* – the surface of wave propagation

is the velocity of transverse waves and

$$K^2 = \frac{e_{15}^2}{\varepsilon_{11}^S C_{44}^E}$$

is the coefficient of electromechanical coupling.

On the basis of expressions (5) and (8) the following expressions for φ and ψ can be written in the form of the Fourier integral:

$$\varphi(X_1, X_2) = \int_{-\infty}^{+\infty} \varphi(k) \exp\{j(\sqrt{-k^2} X_2 + kX_1 - \omega t)\} dk, \tag{9}$$

$$\psi(X_1, X_2) = \int_{-\infty}^{+\infty} \psi(k) \exp\{j(\sqrt{k_t^2 - k^2} X_2 + kX_1 - \omega t)\} dk. \tag{10}$$

From expressions (9) and (10) and the boundary conditions (1) and (2) one can obtain

$$\varphi_{(k)} = -\frac{e_{15}}{\varepsilon_{11}^S} jk\psi(k), \tag{11}$$

$$\psi(k) = \frac{1}{2\pi C_{44}^E k [K^2 \sqrt{-k^2} - \sqrt{k_t^2 - k^2}(1 + K^2)]}. \tag{12}$$

Inserting (12) into (10) and (7) results in an expression for the component of vector particle displacement on the surface $X_2 = 0$,

$$U_{3m}^{(1)} = \frac{j}{2\pi C_{44}^E} \int_{-\infty}^{+\infty} \frac{e^{j(kX_1 - \omega t)}}{F(k)} dk, \tag{13}$$

where

$$F(k) \equiv K^2 \sqrt{-k^2} - \sqrt{k_t^2 - k^2}(1 + K^2). \tag{14}$$

After calculations, one obtains expressions for the component of vector displacement on the surface $X_2 = 0$, for $kX_1 \gg 1$, to a first approximation

$$U_{3m}^{(1)} = -j \frac{K^2}{C_{44}^E (1 + 2K^2)} e^{jk_{BG} X_1} + \ldots \tag{15}$$

The wave number k corresponds in this case to the wave number of the transverse surface wave, for which the designation k_{BG} was introduced.

In the case of a nonmetallized surface the boundary conditions are the

following:

$$T_{23}|_{X_2=0} = C_{44}^E \frac{\partial U_3^{(1)}}{\partial X_2} + e_{15} \frac{\partial \Phi}{\partial X_2} = \delta(X_1) e^{-j\omega t}, \tag{16}$$

$$e_{15} \frac{\partial U_3^{(1)}}{\partial X_2} - \varepsilon_{11}^S \frac{\partial \Phi}{\partial X_2}\bigg|_{X_2=0} = \varepsilon_0 \frac{\partial \Phi'}{\partial X_2} [1 - \delta(X_1)], \tag{17}$$

$$\Phi|_{X_2=0} = \Phi' [1 - \delta(X_1)], \tag{18}$$

where ε_0 is the dielectric constant of a vacuum, and Φ' is the electrical potential in a vacuum, satisfying Laplace's equation

$$\frac{\partial^2 \Phi'}{\partial X_1^2} - \frac{\partial^2 \Phi'}{\partial X_2^2} = 0, \tag{19}$$

$\Phi(X_1, X_2) \to 0$ when $X_2 \to -\infty$.

The remaining symbols are the same as before, using expressions (11) and (12), Φ' in the form

$$\Phi' = \int_{-\infty}^{+\infty} \Phi'(k) \exp\{j(-\sqrt{-k^2} X_2 + kX_1 - \omega t)\} dk, \tag{20}$$

and the boundary conditions (16)-(18), one obtains:

$$\psi(k) = \frac{1}{C_{44}^E 2\pi k} \frac{1}{\dfrac{K^2 \sqrt{-k^2}}{\varepsilon_{11}^S/\varepsilon_0 + 1} - (1+K^2)\sqrt{k_t^2 - k^2}}. \tag{21}$$

Inserting formula (21) into (10) and then into formula (7), one obtains

$$U_3^{(1)} = \frac{j}{2\pi C_{44}^E} \int_{-\infty}^{+\infty} \frac{e^{j(kX_1 - \omega t)}}{F(k)} dk, \tag{22}$$

where

$$F(k) = (1+K^2)(\sqrt{k_t^2 - k^2}) - \frac{K^2 \sqrt{-k^2}}{\varepsilon_{11}^S/\varepsilon_0 + 1}.$$

Using the same method as in the first case, an expression for the vector component of the displacement on the surface $X_2 = 0$ is obtained, which proves the existence of a transverse surface wave of wave number k_{BG},

$$U_3^{(1)} = -\frac{jK^2(1+\varepsilon_{11}^S/\varepsilon_0) e^{jk_{BG}X_1}}{C_{44}^E \{(1+2K^2)(\varepsilon_{11}^S/\varepsilon_0 + 1)^2 + K^4 \varepsilon_{11}^S/\varepsilon_0 (\varepsilon_{11}^S/\varepsilon_0 + 2)}, \tag{23}$$

where

$$k_{GB} = \frac{kt}{[1 - K^4/(1+K^2)^2 \, 1/(1+\varepsilon_{11}^S/\varepsilon_0]^{1/2}}$$

is the wave number of the transverse surface *BG* wave in the case of nonmetallized surface. It can be seen from formulae (15) and (23) that the source generates a surface wave only when the medium is piezoelectric ($K \neq 0$, $U_{31}^{(1)}$, $U_{3m} \neq 0$) The effectiveness of the radiation, as defined by the wave amplitude, depends on the coefficient of electromechanical coupling K (when K changes from 1/3 to 1, U_3 increases by a factor of 3). The effectiveness of the excitation in the case of a source placed on the surface of a metallized medium is about $\varepsilon_{11}/\varepsilon_0$ times greater than in the case of nonmetallized medium. Thus the wave amplitude on a metallized surface is approximately $\varepsilon_{11}^S/\varepsilon_0$ times greater than the wave amplitude on a nonmetallized surface. In the case of lithium iodate $LiIO_3$ the conditions are similar. The difference is that the terms $e_{14}(\partial\Phi/\partial X_1)$ and $e_{14}(\partial U_3/\partial X_2)$ occur in the boundary conditions (1), (16), and (17), and the piezoelectric constant e_{14} enters the expressions for the wave number.

3. A source in the form of vibrating plate on the surface of wave propagation

The coordinate system is shown in Fig. 2. In the case of a metallized surface, the boundary conditions are the following:

$$T_{23}|_{X_2=0} = C_{44}^E \frac{\partial U_{3m}^{(2)}}{\partial X_2} + e_{15} \frac{\partial \Phi}{\partial X_2} = \begin{cases} 0, & |X| > a, \\ e^{-j\omega t}, & |X| \leqslant a, \end{cases} \tag{24}$$

$$\Phi|_{X_2=0} \equiv 0, \quad \frac{e_{15}}{\varepsilon_{11}^S} U_{3m}^{(2)} + \varphi|_{X_2=0} \equiv 0. \tag{25}$$

Using a similar calculation method, one can obtain the following formulae for the vector component of particle displacement on the surface $X_2 = 0$:

$$U_{3m}^{(2)} = -\frac{j2K^2}{C_{44}^E(1+2K^2)} \frac{\sin k_{BG}}{k_{BG}} \exp\{jk_{BG}X_1\}. \tag{26}$$

While for a nonmetallized surface one obtains:

$$U_3^{(2)} = \frac{2jK^2(1+\varepsilon_{11}^S/\varepsilon_0)\dfrac{\sin K_{BG}}{k_{BG}} \exp\{jk_{BG}X_1\}}{k_{BG}C_{44}^E\{(1+2K^2)(\varepsilon_{11}^S/\varepsilon_0+1)^2+K^2(\varepsilon_{11}^S/\varepsilon_0)(\varepsilon_{11}^S/\varepsilon_0+2)\}} + \ldots \tag{27}$$

It can be seen from formulae (26) and (27) that the conclusions for the first case are also valid for this case. The dependence of the amplitude of the transverse *BG* wave on the width of the surface of the source also occurs. Maxima and minima of the amplitude are seen, depending on the width of the source a. When

$$a = \frac{2n+1}{k_{BG}} \frac{\pi}{2}, \quad n = 0, 1, 2, \ldots, \tag{28}$$

the amplitude is a maximum, and when

$$a = \frac{n}{k_{BG}^2}\frac{\pi}{2}. \tag{29}$$

4. A source in the form of plate vibrating on a surface perpendicular to the surface of wave propagation

The coordinate system is shown in Fig. 3. It is assumed that the *BG* wave propagates from the surface $X_1 = 0$ to the surface $X_2 = 0$ with a certain transmission coefficient N. In this case a change of the energy of the transverse wave into the energy of *BG* wave occurs close to the line at which the surface $X_2 = 0$ crosses the surface $X_1 = 0$.

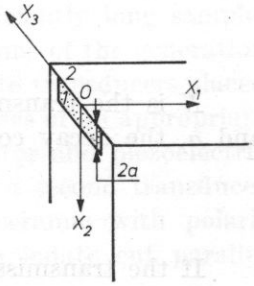

Fig. 3. A plate source on the surface perpendicular to the surface of wave propagation
1 – plate source, *2* – the surface of wave propagation

If the surface is metallized, two sources of strain are placed on the surface $X_2 = 0$, satisfying the following boundary conditions; for the first source

$$T_{23}|_{X_2=0} = C_{44}^E \frac{\partial U_{3m}^{(3)}}{\partial X_2} + e_{15}\frac{\partial \Phi}{\partial X_2} = \delta(X_1)\left(\frac{1-e^{-2a a}}{a}\right)e^{-j\omega t}, \tag{30}$$

where a is a coefficient of decay. It is assumed that it is equal to the decay coefficient of the *BG* wave, i.e.

$$\frac{K^2}{1+K^2}k_{BG}, \tag{31}$$

$$\Phi|_{X_2=0} \equiv \frac{e_{15}}{\varepsilon_{11}^S} U_{3m}^{(3)} + \varphi|_{X_2=0} = 0. \tag{32}$$

For the second source

$$T_{23}|_{X_2=0} = C_{44}^E \frac{\partial U_{3m}^{(3)}}{\partial X_2} + e_{15}\frac{\partial \Phi}{\partial X_2} = \begin{cases} 0, & x > 2a,\ x < 0, \\ Ne^{-j\omega t}, & x \leqslant 2a, \end{cases} \tag{33}$$

$$\Phi|_{X_2=0} \equiv \frac{e_{15}}{\varepsilon_{11}} U_{3m}^{(3)} + \varphi|_{X_2=0} = 0. \tag{34}$$

After calculation, the following results are obtained for the vector compo-

nent of particle displacement on the surface $X_2 = 0$:

$$U_{3m}^{(3)} = -\frac{j2K^2}{C_{44}(1+2K^2)}\left[\left(\frac{1-e^{2\alpha a}}{\alpha}\right)p\right]e^{jk_{BG}X_1}, \tag{35}$$

where

$$p = \left|\frac{1}{jk_{BG}}(e^{jk_{BG}2a}-1)N'\right|, \tag{36}$$

and N' is the transmission coefficient in the case of metallized surface.

For a nonmetallized surface one obtains

$$U_3^{(3)} = \frac{-jK^2(1+\varepsilon_{11}^S/\varepsilon_0)e^{jk_{BG}X_1}}{C_{44}^E\{(1+2K^2)(\varepsilon_{11}^S/\varepsilon_0-1)^2+K^4(\varepsilon_{11}^S/\varepsilon_0)(\varepsilon_{11}^S/\varepsilon_0-2)}, \tag{37}$$

where

$$p' = \left|\frac{1}{jk_{BG}}(e^{jk_{BG}2a}-1)\right|N. \tag{38}$$

N is the transmission coefficient in the case of a nonmetallized surface, and α, the decay coefficient, is given by

$$\alpha' = \frac{K^2}{(1+K^2)(1+\varepsilon_{11}^S/\varepsilon_0)}k_{BG}. \tag{39}$$

If the transmission coefficients N and N' are very low, the second term in formulae (35) and (37) can be neglected. Then the amplitude of the BG wave on the surface $X_2 = 0$ is inversely proportional to the decay coefficient $U_{3m}^{(3)} \sim \sim 1/\alpha$, $U_3^{(3)} \ll 1/\alpha'$. Thus the optimum transducer height is given by:

$$2a_{\text{opt}} = \frac{1}{\alpha} \quad \text{(metallized)},$$

$$2a'_{\text{opt}} = \frac{1}{\alpha} \quad \text{(nonmetallized)}.$$

For $\alpha' \ll \alpha$ and $a'_{\text{opt}} \gg a_{\text{opt}}$, the ratio of the amplitude interfering bulk wave to that of the BG wave is very large in the case of a nonmetallized surface, and thus the excitation effectiveness of the wave is very small.

If the transmission coefficients N and N' are large, the first terms in formulae (35) and (37) can be neglected, and the amplitude of the BG wave on the surface $X_2 = 0$ is proportional to p or p', i.e. it depends on the width of the source.

5. Experimental methods for the generation and detection of transverse waves

It follows from the theoretical investigations that the transverse surface wave in the case of a free surface penetrates in the piezoelectric material and has a velocity close to the velocity of the bulk wave, so that in practice the two waves cannot be distinguished [6]. Covering the propagation surface with a

thin and weightless conductor changes the conditions of wave propagation in favour of the surface wave. A rise in the pulse transmitted by this wave and a decrease in the wave propagation velocity can be observed. This is caused by a formation on the surface of the piezoelectric material, of a layer of decreased stiffness, due to the compensation of the inner piezoelectric field. The experimental investigation of the generation and propagation of transverse surface waves is usually performed in the presence of a conducting surface, but even with a conducting surface, the separation of the surface *BG* wave from the bulk *SH* wave is a difficult but vital problem, which is not always appreciated by experimentors. This problem also occurs in the use of interdigital (IDT) transducers [8], and the impossibility of differentiating the pulses of the *BG* and *SH* waves can lead to incorrect conclusions.

As a result of a small difference in velocity, the separation of pulses of *BG* and *SH* waves can be achieved in the case of a sufficiently long sample. In the experimental phase of the present work, investigations of the generation and detection of the surface wave were performed using plate transducers placed on the sides of the sample as shown in Fig. 3. Acoustic pulses of an appropriate frequency were generated using an electrical pulse generator and piezoelectric transducers. The presence of the waves was detected by a second transducer connected to an oscilloscope. Samples of piezoelectric ceramic with polarisation parallel to the propagation plane, and of lithium iodate cut parallel to the z axis, were used in the investigations.

The presence of the *BG* wave can be found by exerting mechanical pressure on the surface of wave propagation or better still by covering this surface with viscous resin. The pressure causes damping of the *BG* pulse (Fig. 4) which is not observed in the bulk wave. In the case a conductive surface, the surface wave propagates in the layer below the surface, while the bulk *SH* wave propagates more deeply. This phenomenon can be used for the separation of the pure *BG* wave.

It was found possible to obtain a separated, pure transvers surface *BG* wave on the samples of piezoelectric material, with a dimension of 46 mm, using piezoelectric transducers contiguous to the sample along a line (Fig. 5). This contact can be considered as a linear wave source, and it can also be realized by a slight inclination of the lateral planes of the sample.

It can be seen from Fig. 6 that the surface wave is almost completely attenuated by the viscous resin placed on the propagation surface. However, in the case of a nonmetallized surface, only the bulk *SH* wave occurs in practice and it is not attenuated by the resin, Fig. 6.

The excitation of the *BG* wave by a transducer placed on the propagation surface is shown in Fig. 7. Moving the transmitting transducer over the surface causes the position of the pulse on the time axis of the oscilloscope to shift in direct proportion to the path length of the wave. The measured wave velocity shows that a surface (*BG*) wave occurs.

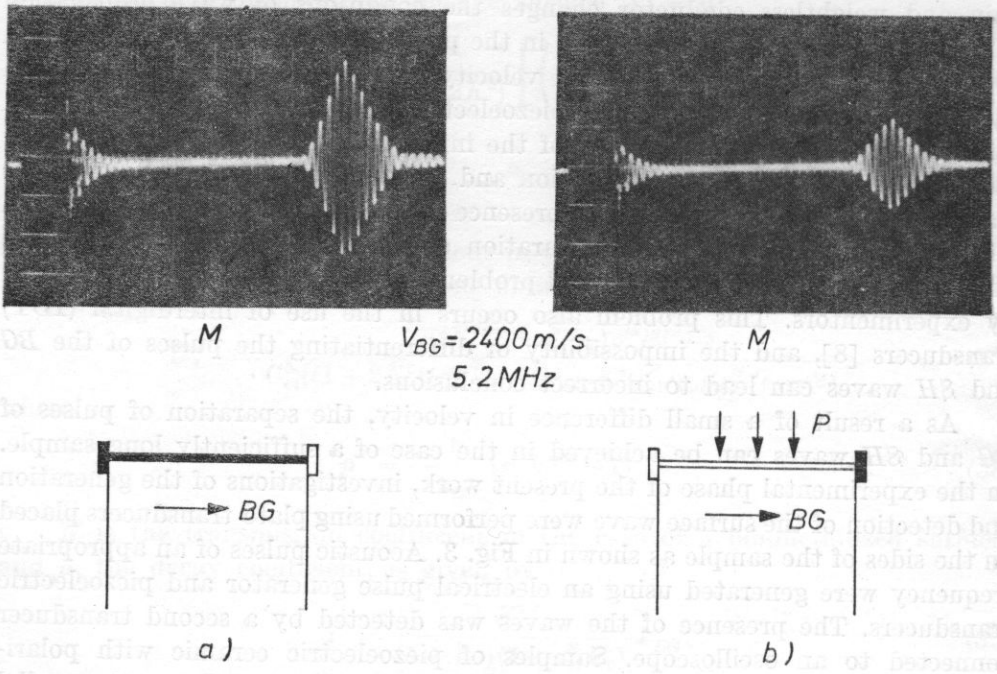

Fig. 4. The effect of pressure on the amplitude of the transverse surface wave on lithium iodate with a metallized surface

a – the pulse without loading on the surface, b – the pulse on the loaded surface

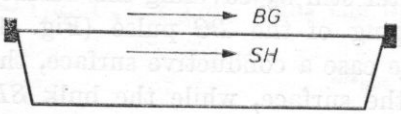

Fig. 5. The manner of exciting a pure acousto-electrical (*BG*) wave of a piezoelectric ceramic

Generally, separation of the transverse surface (*BG*) wave is easier in lithium iodate. This is connected with the properties of the surface layer. In this case, this layer seems to reach deeper and in this connection the transducer generating the wave is within the region of the surface layer.

6. Conclusions

It follows from the theoretical consideration and from the measurements performed, that it is possible to obtain pulses of pure transverse surface waves using plate transducers, despite the fact that the velocity of the surface wave is only slightly different from the velocity of the bulk wave, and superposition of the pulses can occur with short samples and wide transducers. Excitation of surface waves with plate transducers is relatively easy and can be used in the investigation of new piezoelectric materials, and of those materials whose surface layers are changed by technological processes [11]. Separation of pure surface waves is also significant in the investigation of their properties [10].

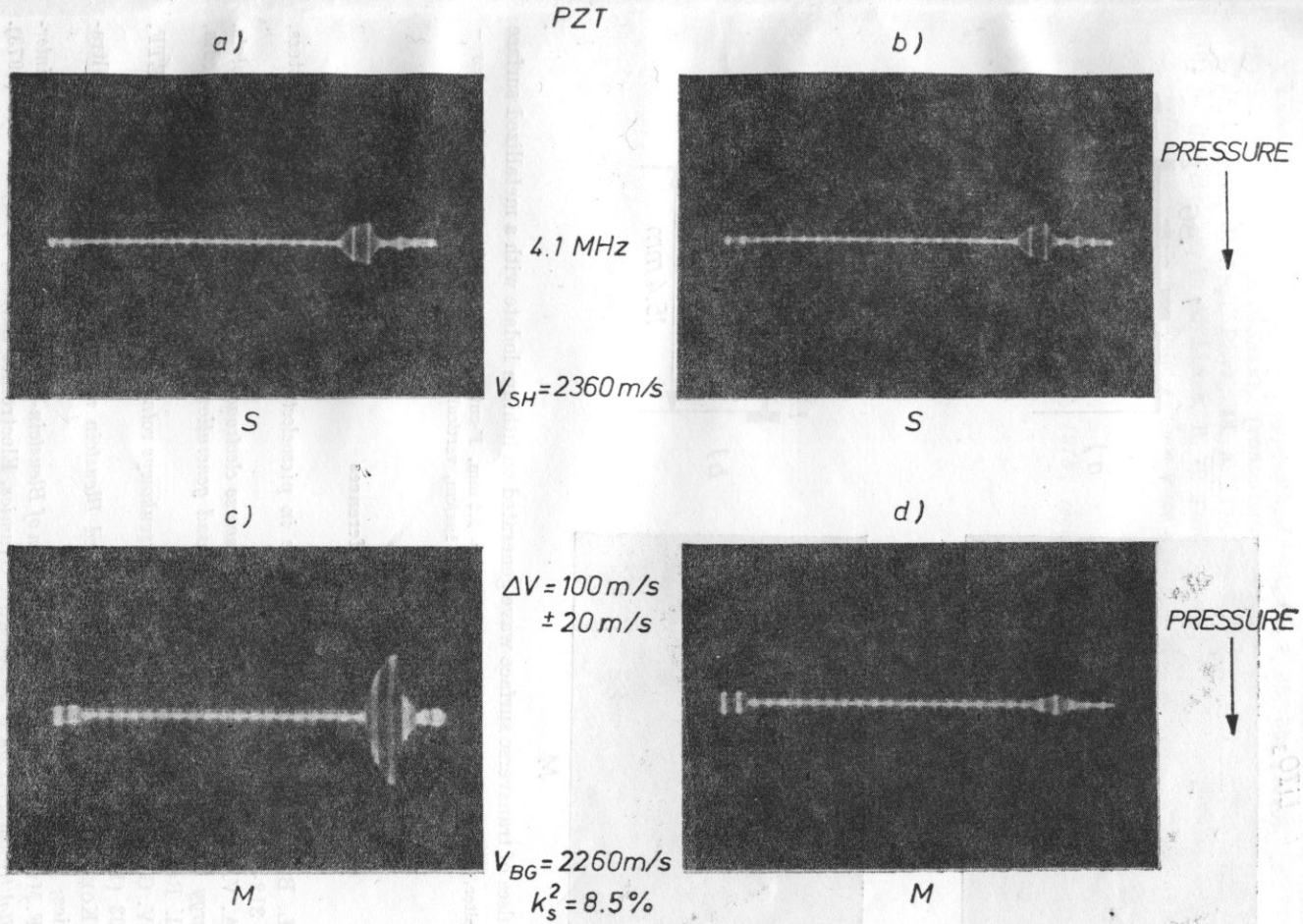

Fig. 6. Pulses of the transverse bulk wave (a-b) and acoustoelectric *BG* wave (c-d) at a frequency of 4.1 MHz excited as in Fig. 5

a – a nonmetallized ceramic surface, b – a nonmetallized surface loaded with a liquid resin, c – a metallized surface, d – a metallized surface loaded with resin indices in 1μs, voltage in 0.5 × 0 V/cm

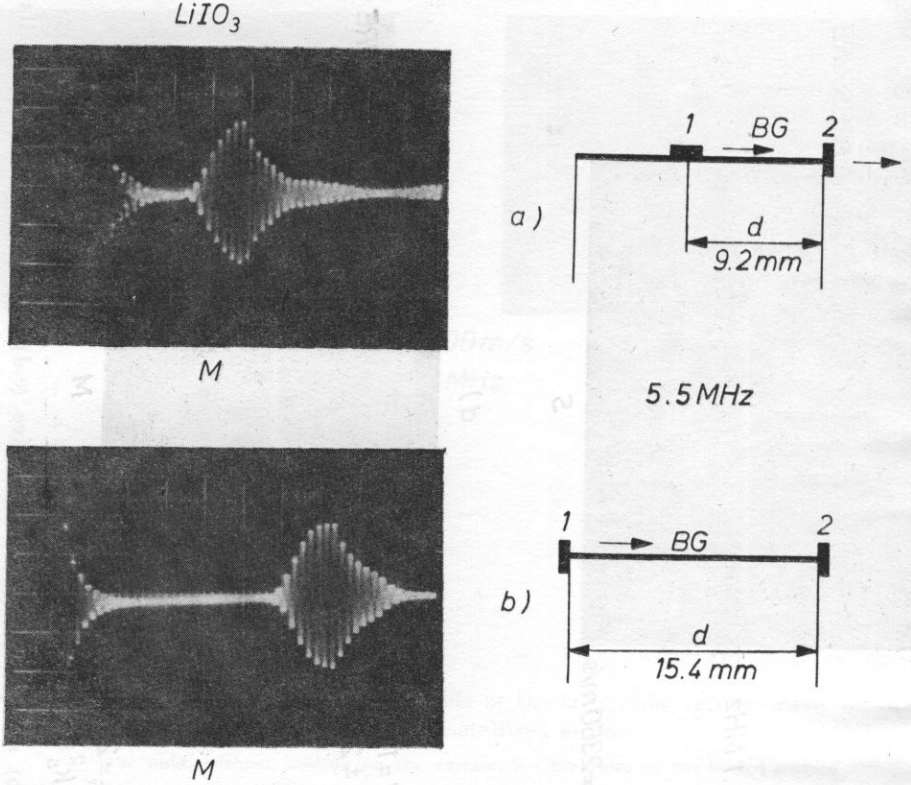

Fig. 7. Pulses of transverse surface wave generated on lithium iodate with a metallized surface
1 – transmiter, *2* – receiver, $d = 4.6$ mm, (3-4) $d = 9.2$ mm, *Y*-cut, propagation direction *X*, frequency – 5.5 MHz, horizontal scale 1μs/cm, vertical scale 0.1 V/cm

References

[1] T. L. Bleustein, *A new surface wave in piezoelectric materials*, Appl. Phys. Letters, **13**, 312-313 (1968).

[2] P. A. Van Dalen, *Propagation of transverse electroacoustic waves in a piezoelectric plate. Energy considerations on propagation and generation of A.S.W. in piezoelectric media*, Phil. Res. Repts., **27**, 4 (1972).

[3] U. V. Gulayev *Powerkhnostnye electrozvukowye volny w twiordykh telakh*, Pisma ŻETF, **2**, 63 (1969).

[4] G. Koerber, R. F. Vogel, *Generalized Bleustein modes*, IEEE Trans. Sonios, Ultrasonics, **SU-19** 1, 3-8 (1972).

[5] M. F. Milson, M. Reedwood, *Generation of Bleustein-Gulayev and bulk shear waves by interdigital transducers on a piezoelectric ceramics*, Electronics Letters, **9**, 18, 417-419 (1973).

[6] E. G. S. Paige, E. G. Marschall, *Novel acoustic surface wave directional coupler with diverse applications*, Electronics Letters, **7**, 460-462 (1971).

[7] W. Pajewski, *Transverse Bleustein-Gulayer (B.G.) surface waves on a piezoelectric ceramic*, Arch. Akustyki, **12**, 3-235-243 (1977).

[8] H. A. SABBAGH, T. F. KRILE, *Excitation, detection and scattering of electroelastic surface waves via an integral equation approach*, JASA, **60**, 3, 626-633 (1976).

[9] K. TANAKA, Z. KAWASAKI, *Transmission characteristics of Bleustein-Gulayev waves at a corner*, J. Appl. Phys., **48**, 5, 1778-1782 (1977).

[10] B. R. TITTMAN, C. A. ALERS, R. B. THOMPSON, R. A. JONG, *Characterisation of subsurface anomalies by elastic surface wave dispersion*, 1975 Ultrasonic Symposium Proceedings IEEE, pp. 561-564.

Received on May 22, 1978; revised version on March 1, 1980.